What controls the mesoscale variations in water isotopic composition within tropical cyclones and squall lines? Cloud resolving model simulations

Camille Risi[1], Caroline Muller[2], Françoise Vimeux[3], Peter N. Blossey[4], Grégoire Védeau[5], Clarisse Dufaux[5], and Sophie Abramian[6]

[1]LMD, IPSL, CNRS, Paris, France
[2]LMD/ENS
[3]IRD
[4]University of Washington
[5]Laboratoire de Meteorologie Dynamique
[6]Laboratoire de Météorologie Dynamique

November 24, 2022

Abstract

One way to test our understanding of the impact of convective processes on the isotopic composition of water vapor and precipitation is to analyze the isotopic mesoscale variations during organized convective systems such as tropical cyclones or squall lines. The goal of this study is to understand these isotopic mesoscale variations with particular attention to isotopic signals in near-surface vapor and precipitation that may be present in observations and in paleoclimate proxies. With this aim, we run cloud resolving model simulations in radiative-convective equilibrium in which rotation or wind shear is added, allowing us to simulate tropical cyclones or squall lines. The simulations capture the robust aspects of mesoscale isotopic variations in observed cyclones and squall lines. We interpret these variations using a simple water budget model for the sub-cloud layer of different parts of the domain. We find that rain evaporation and rain-vapor diffusive exchanges are the main drivers of isotopic depletion within cyclones and squall lines. Horizontal advection spreads isotopic anomalies, thus reshaping the mesoscale isotopic pattern. Variations in near-surface relative humidity and wind speed have a significant impact on d-excess variations within tropical cyclones, but the evaporation of sea spray is not necessary to explain the observed enrichment in the eye. This study strengthens our understanding of mesoscale isotopic variability and provides physical arguments supporting the interpretation of paleoclimate isotopic archives in tropical regions in terms of past cyclonic activity.

What controls the mesoscale variations in water isotopic composition within tropical cyclones and squall lines? Cloud resolving model simulations

Camille Risi [1], Caroline Muller [1], Françoise Vimeux [2,3], Peter Blossey [4], Grégoire Védeau [1,3], Clarisse Dufaux [1], Sophie Abramian [1]

[1]Laboratoire de Meteorologie Dynamique, IPSL, CNRS, Ecole Normale Superieure, Sorbonne Universite, PSL Research University, Paris, France
[2] HydroSciences Montpellier (HSM), UMR 5569 (UM, CNRS, IRD), 34095 Montpellier, France
[3]Institut Pierre Simon Laplace (IPSL), Laboratoire des Sciences du Climat et de l'Environnement (LSCE), UMR 8212 (CEA, CNRS, UVSQ), 91191 Gif-sur-Yvette, France
[4]Department of Atmospheric Sciences, University of Washington, Seattle, USA

Key Points:

- Cloud resolving model simulations capture robust aspects of mesoscale isotopic variations in observed cyclones and squall lines
- Rain evaporation and rain-vapor diffusive exchanges are the main drivers of isotopic depletion within cyclones and squall lines
- Horizontal advection spreads isotopic anomalies, thus reshaping the mesoscale isotopic pattern

Corresponding author: Camille RISI, `Camille.Risi@lmd.ipsl.fr`

Abstract

One way to test our understanding of the impact of convective processes on the isotopic composition of water vapor and precipitation is to analyze the isotopic mesoscale variations during organized convective systems such as tropical cyclones or squall lines. The goal of this study is to understand these isotopic mesoscale variations with particular attention to isotopic signals in near-surface vapor and precipitation that may be present in observations and in paleoclimate proxies. With this aim, we run cloud resolving model simulations in radiative-convective equilibrium in which rotation or wind shear is added, allowing us to simulate tropical cyclones or squall lines. The simulations capture the robust aspects of mesoscale isotopic variations in observed cyclones and squall lines. We interpret these variations using a simple water budget model for the sub-cloud layer of different parts of the domain. We find that rain evaporation and rain-vapor diffusive exchanges are the main drivers of isotopic depletion within cyclones and squall lines. Horizontal advection spreads isotopic anomalies, thus reshaping the mesoscale isotopic pattern. Variations in near-surface relative humidity and wind speed have a significant impact on d-excess variations within tropical cyclones, but the evaporation of sea spray is not necessary to explain the observed enrichment in the eye. This study strengthens our understanding of mesoscale isotopic variability and provides physical arguments supporting the interpretation of paleoclimate isotopic archives in tropical regions in terms of past cyclonic activity.

Plain Language Summary

Water molecules can be light (one oxygen atom and two hydrogen atoms) or heavy (one hydrogen atom is replaced by a deuterium atom). These different molecules are called water isotopes. In large, long-lived, severe storms such as tropical cyclones or squall lines (thunderstorms that organize into lines), the rain is observed to be more depleted in heavy isotopes. Several studies have exploited this property to reconstruct the past variations in the frequency of occurence of tropical cyclones or severe thunderstorms based on isotope variations observed in speleothems. The aim of this study is to understand what controls the depletion of the rain in tropical cyclones and squall lines. With this aim, for the first time we use high-resolution simulations (2-4 km in horizontal) to simulate the internal dynamics of tropical cyclones and squall lines and their isotope composition. We design a simple model to interpret the results. We show that the depletion in heavy isotopes of the rain is mainly due to rain evaporation, which moistens the lower atmosphere with depleted water vapor.

1 Introduction

The isotopic composition of water vapor (HDO or $H_2^{18}O$) evolves along the water cycle as phase changes are associated with isotopic fractionation. The isotopic composition of precipitation recorded in paleoclimate archives has significantly contributed to the reconstruction of past hydrological changes across the tropics (Wang et al., 2001; Cruz et al., 2009). Indeed, over tropical oceans, the precipitation is usually more depleted in heavy isotopes as precipitation rate increases, an observation called the amount effect (Dansgaard, 1964). In concert with the precipitation, the water vapor over tropical oceans is also more depleted as precipitation rate increases according to satellite and in-situ observations (Worden et al., 2007; Kurita, 2013). Over tropical land, both the precipitation and water vapor are generally observed to be more depleted as the precipitation rate increases in average over the previous days before the observation of isotopic depletion and in average over some large-scale domain upstream of the region of depletion, for example in Western Africa (Risi et al., 2008; Tremoy et al., 2012), Southeast Tibetan Plateau (Gao et al., 2013), Southern India (Lekshmy et al., 2014; Sinha & Chakraborty, 2020), Southern tropical America (Vimeux et al., 2005; Vimeux et al., 2011) or the Maritime Continent (Moerman et al., 2013; Conroy et al., 2016). In the tropics, the importance of precipitation rate, either at the local or at the regional scale, in controlling the water isotopic composition of water vapor and precipitation is thus well established. However, the relationship between the water isotopic composition and precipitation rate can vary temporally and spatially. For example, it may depend on the proportion of stratiform versus convective rain (Aggarwal et al., 2016), on the organization of convection (Lawrence et al., 2004; Risi et al., 2008; Chakraborty et al., 2016) or on the shape of vertical velocity profiles (Moore et al., 2014; Torri et al., 2017; Lacour et al., 2017). For a more robust and quantitative interpretation of water isotopic archives in terms of past hydrological changes or cyclonic activity, a better understanding of how the precipitation rate impacts the isotopic composition of water vapor and precipitation is thus necessary.

In the tropics, the main source of precipitation is deep convection (Houze, 2004). It is associated with processes which deplete the water vapor in heavy isotopes. In particular, observational studies have highlighted the role of rain evaporation (Worden et al., 2007), diffusive liquid vapor exchanges (Lawrence et al., 2004), meso-scale downdrafts (Risi et al., 2010; Kurita, 2013) and microphysical processes in stratiform regions of convective systems (Aggarwal et al., 2016). Modeling studies with high resolution simulations have confirmed the key role of rain evaporation and of microphysical processes in stratiform regions of convective systems, especially melting of depleted snow that subsequently evaporates (Risi et al., 2021).

One way to test the importance of these processes is to investigate the observed evolution of the isotopic composition of precipitation or near-surface water vapor within "organized" convective systems (Risi et al., 2010). By organized, we mean that the convective system has different parts, characterized by different convective or microphysical processes, and connected through some meso-scale circulation. For example, squall lines are elongated, propagative convective systems with a gust front in front, followed by a convective region of intense rainfall, a transition region with a paused rainfall, and a trailing stratiform region of light rainfall (Houze, 2004). The precipitation collected during squall lines often features a W shape with more depleted rain in convective and stratiform regions (Taupin & Gallaire, 1998; Risi et al., 2010). In the near-surface water vapor, many squall lines show isotopic depletion in the convective and stratiform regions (Tremoy et al., 2014). This pattern has been interpreted in terms of rain evaporation and meso-scale downdrafts.

As another example, tropical cyclones are a spectacular manifestation of convective organization, with usually an eye at the center, surrounded by convective walls with very intense rainfall and spiral rain bands reaching several hundreds of kilometers (Houze, 2010). The precipitation and near-surface water vapor collected in the vicinity of tropical cyclones often show stronger depletion towards the cyclone center, more depleted water vapor in spiral bands than in between bands (Gedzelman et al., 2003; Xu et al., 2019), and more enriched water vapor in the eye (Fudeyasu et al., 2008). The depletion has been interpreted in terms of progressive rain out towards the center and rain-vapor diffusive exchanges (J. R. Lawrence et al., 2002). The enrichment in the eye has been interpreted in terms of sea spray evaporation (Fudeyasu et al., 2008).

The goal of this paper is to investigate the processes controlling the evolution of near-surface water vapor and precipitation within squall lines and tropical cyclones. So far, this question has often been addressed using observational studies or simple conceptual models. Here for the first time, we use three-dimensional high-resolution, isotope-enabled simulations in which convective motions are explicitly represented. Using these simulations together with an interpretative framework, we aim at quantifying the relative importance of the different processes that have been previously suggested in the literature. Our simulations will be run in idealized conditions of radiative-convective equilibrium. Therefore, we will focus on robust features that are observed in most squall lines and tropical cyclones based on previous studies. No one-to-one comparison can be made with any particular real observed system.

This study may also be useful to better understand how convective organization could be recorded in paleoclimate archives. In particular, more organized convective systems, such as squall lines (Risi et al., 2008; Tremoy et al., 2014; Maupin et al., 2021) or tropical cyclones (J. R. Lawrence & Gedzelman, 1996; Lawrence et al., 2004; Price et al., 2008; Chakraborty et al., 2016), have been observed to be associated with water vapor and precipitation that are more depleted in heavy isotopes than unorganized systems. Inparticular, the depleted rain of tropical cyclones leaves a depleted imprint in surface waters and can significantly affect long-term averages of isotopic composition of precipitation or surface waters (J. R. Lawrence, 1998; Baldini et al., 2016). This suggests that the isotopic composition of precipitation recorded in speleothems could be used to reconstruct past cyclonic activity (J. Lawrence & Gedzelman, 2003; Frappier et al., 2007; Chen et al., 2021). In the past few years, several studies have interpreted speleothems in terms of cyclonic frequency (Nott et al., 2007; Medina-Elizalde & Rohling, 2012; Baldini et al., 2016). Similarly, the depletion observed in Texan speleothems has been interpreted as enhanced activity of large, long-lived, organized convective systems (Maupin et al., 2021).

2 Model and simulations

2.1 Isotopic variables

The water content in heavy isotopes (HDO or $H_2^{18}O$) is expressed in ‰ as $\delta D = (R_D/R_{D,SMOW} - 1) \times 1000$ and $\delta^{18}O = \left(R_{^{18}O}/R_{^{18}O,SMOW} - 1\right) \times 1000$, where R_D and $R_{^{18}O}$ are the ratio of Deuterium over Hydrogen atoms and of ^{18}O over ^{16}O atoms in the water, and SMOW is the Standard Mean Ocean Water reference. To first order, δD variations are 8 times those in $\delta^{18}O$ (Craig, 1961), so we will focus on δD here. However, slight deviations in the $\delta D - \delta^{18}O$ relationship can be quantified by the second-order parameter d-excess: $d = \delta D - 8 \cdot \delta^{18}O$. It reflects kinetic effects, i.e. associated with diffusivity differences between the different water isotopologues. We will also show some results for d-excess as it can reflect kinetic effects in rain evaporation or surface evaporation.

2.2 Cloud Resolving Model

We use the same Cloud Resolving Model (CRM) as in (Risi et al., 2020), namely the System for Atmospheric Modeling (SAM) non-hydrostatic model (M. F. Khairoutdinov & Randall, 2003), version 6.10.9, which is enabled with water isotopes (Blossey et al., 2010). This model solves anelastic conservation equations for momentum, mass, energy and water, which is present in the model under six phases: water vapor, cloud liquid, cloud ice, precipitating liquid, precipitating snow, and precipitating graupel. We use the bulk, mixed-phase microphysical parameterization from Thompson et al. (2008) in which water isotopes were implemented (Moore et al., 2016).

At the ocean surface, there is no representation of sea spray. Therefore, we do not expect to simulate the possible impact of sea spray on the isotopic composition in the eye (Fudeyasu et al., 2008).

2.3 Radiative-convective equilibrium with large-scale forcing

Simulations are three-dimensional, with a doubly-periodic domain. They are run in radiative-convective equilibrium over an ocean surface. The sea surface temperature (SST) is 30°C. There is no diurnal cycle.

Organized convection is typically observed in regions of large-scale ascent (Tan et al., 2013; Jakob et al., 2019). Therefore, we impose a large-scale vertical ascent with a cubic shape, reaching -60 hPa/d at 500 hPa and 0 hPa/d at the surface and above 100 hPa (Risi et al., 2020).

Simulations were also run without vertical ascent, and gave similar results except that the convective systems were smaller and with a less defined internal structure. For example, the tropical cyclone without ascent does not show any eye at the center. We thus focus on the simulations with large-scale ascent in the following.

The simulations are run during 50 days. The last 10 days of simulation are analyzed with one three-dimensional output file every day.

2.4 Set-up for the cyclone simulation

We use a domain of 1024 km×1024 km with a horizontal resolution of 4 km and 96 vertical levels. This horizontal resolution is sufficient to properly simulate the internal structure of a cyclone (Gentry & Lackmann, 2010). Cyclones spontaneously develop in radiative-convective equilibrium simulations when some rotation is added (M. Khairoutdinov & Emanuel, 2013; C. J. Muller & Romps, 2018). Here the effect of rotation is added through a Coriolis parameter that corresponds to a latitude of 40°. Although no tropical cyclones are expected to form at such latitudes, a strong rotation allows us to simulate a small cyclone (Chavas & Emanuel, 2014) that can fit our small domain. This allows the simulation to remain computationally reasonable.

The initial conditions are spatially homogeneous and one unique cyclone develops spontaneously through self-aggregation mechanisms after a few days. This is consistent with the time scale for cyclogenesis in other self-aggregation studies (C. J. Muller & Romps, 2018).

2.5 Set-up for the squall line simulation

We use a domain of 256 km×256 km with a horizontal resolution is 2 km and 96 vertical levels. Squall lines spontaneously develop in radiative-convective equilibrium simulations when horizontal wind shear is added (Robe & Emanuel, 2001; C. Muller, 2013). We add a horizontally uniform wind in the x direction that reaches 10 m/s at the surface and linearly decrease to 0 m/s at 1 km. According to (Rotunno et al., 1988), this critical shear with our settings leads to the formation of a strong and long-lived squall line, perpendicular to the background wind. The uniform surface wind is subtracted when calculating surface fluxes, to avoid this simulation to have significantly higher surface fluxes. The radiative fluxes are imposed, because interactive radiation leads to some radiative feedbacks that disfavors the organization into squall lines.

The convection quickly organizes into a line, after about one day of simulation.

3 Simulated patterns and qualitative comparison with observations

3.1 Tropical cyclone

3.1.1 Meso-scale structure

To visualize the meso-scale structure of the tropical cyclone, in Figure 1 we plot maps of precipitation rate, near-surface air temperature, surface pressure anomaly, near-surface relative humidity, near-surface water vapor δD and surface rain δD for an arbitrary snapshot. The simulated cyclone exhibits features that are typical of observed cyclones (Houze, 2010). It exhibits a small eye with weak precipitation (Figure 1a) and warm air (Figure 1b), consistent with the subsidence in the eye. It is surrounded by an eyewall and spiraling rain bands with very intense precipitation and strong cyclonic winds. Around the cyclone, strong compensating subsidence develops, leading to a very dry environment and some scattered, isolated cumulus and cumulonimbus clouds and their cold pools (Figure 1a-b,d).

To better document the different parts of the tropical cyclone, we plot composites of meteorological and isotopic variables as a function of the distance r to the storm center (Figure 2 and 3). All 10 snapshots were used to compute the composites. The storm center is defined as the minimum surface pressure over the domain for each snapshot. The typical structure of a tropical cyclone is well captured.

- The eye is associated with minimum pressure (around 50hPa lower than in the environment, typical of category 4 cyclones), a local minimum in precipitation, maximum nea-surface air temperature and relative humidity and weak winds (Figure 2a-c). The eye is however to small to see the expected subsidence in Fig 2.
- The eyewall is associated with maximum precipitation and horizontal winds. The air is strongly ascending, almost saturated throughout the full troposphere (Figure 3a), and condensation is very intense except in the shallow sub-cloud layer (Figure 3c).
- Beyond the eyewall, rain bands are associated with significant but weaker precipitation and winds. There is strong condensation, but the air is in average drier (Figure 3a), allowing thick layers of snow sublimation and rain evaporation (Figure 3c).

3.1.2 Definition of sub-domains

Based on the previous description of meso-scale structure, we divide all grid points into 5 sub-domains. These sub-domains are defined automatically based on some arbitrary thresholds, to which results are not crucially sensitive. We define:

- the "eye" as grid points for which $r \leq r_{wall}$, where r_{wall} is the first r value for which the precipitation exceeds 20 times the domain-average precipitation (yellow rectangles in Figure 2).
- the "eyewall" as grid points for which $r_{wall} < r \leq r_{band}$, where r_{band} is the first r value for which $r > r_{wall}$ and the precipitation is lower than 20 times the domain-average precipitation (blue rectangles in Figure 2).
- the "environment" as grid points for which $r > r_{env}$, where r_{env} is the first r value for which $r > r_{band}$ and the precipitation is lower than 0.8 times the domain-average precipitation (left in white in Figure 2).

In between the eyewall and the environment (pink rectangles in Figure 2), rain bands are not radially symmetric. Therefore, we define "rain bands" as grid points for which $r_{band} < r \leq r_{env}$ and precipitation exceeds 4 times the domain-average precipitation, and "in between rain bands" as the other points.

3.1.3 Simulated isotopic evolution

The water vapor is most enriched in the eye and in the dry environment (Figure 1e-f, Figure 2e), and most depleted in the eyewall and spiraling rain bands. The water vapor d-excess is lower in the eye, and higher in the eyewall and rain bands (2e-f). Areas in-between rain bands are associated with weaker depletion and higher d-excess (Figure 2d-e, dashed black) than in rain bands.

The precipitation δD (δD_p) varies in concert with the water vapor δD (δD_v) where the precipitation is highest (Figure 2e, dashed black). The precipitation is slightly more

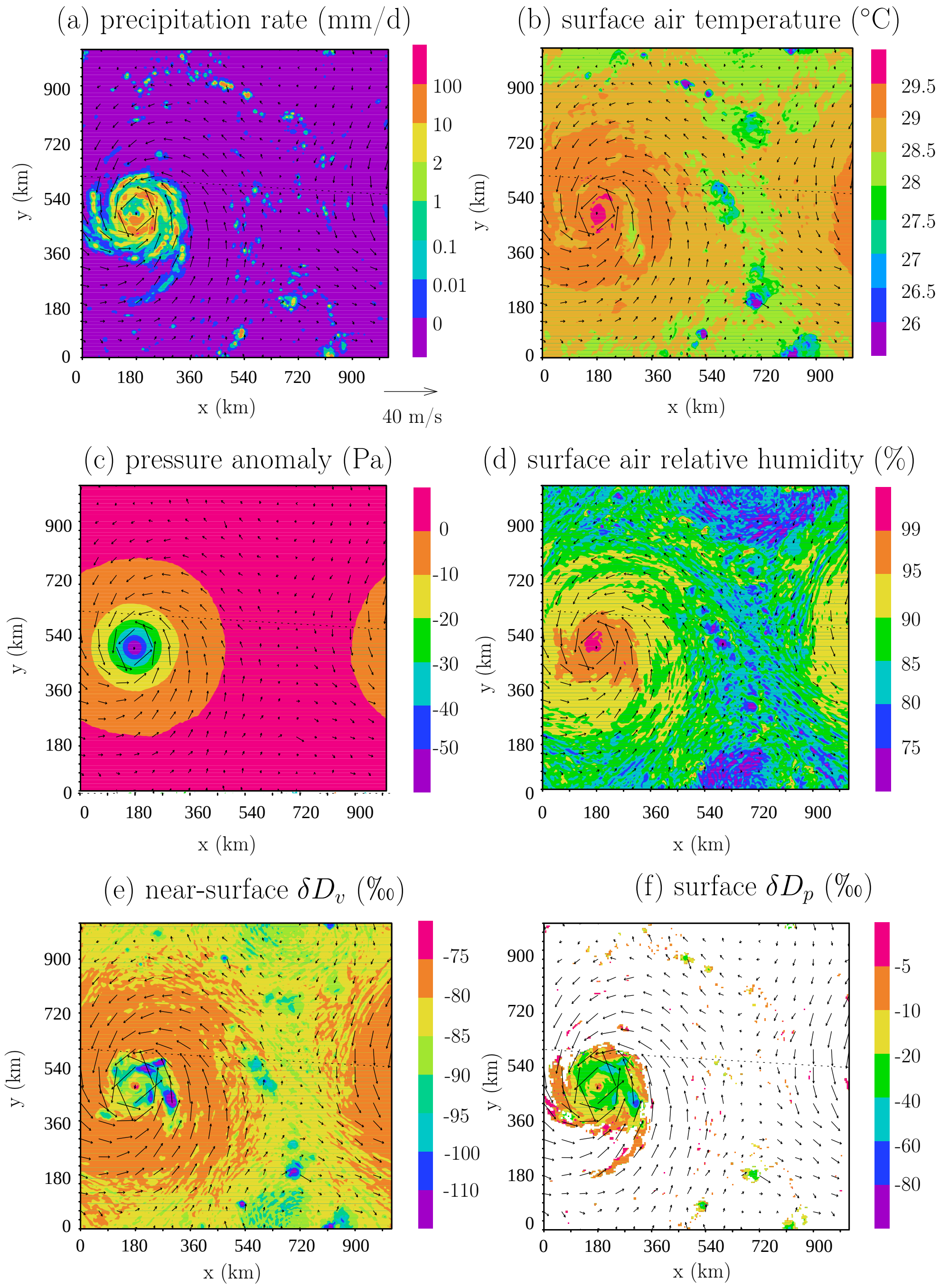

Figure 1. Maps for a snapshot of the cyclone simulation: (a) precipitation rate, (b) near-surface air temperature, (c) surface pressure anomaly with respect to the domain-mean, (d) near-surface relative humidity, (e) near-surface δD_v and (f) δD_p. The near surface winds are shown as arrows. Note that due to the doubly-periodic domain, the missing part of the cyclone on the left edge of the domain appears on the right edge of the domain. The snapshot was chosen as the one where the cyclone is the closest to the center of the domain, for easier visualization.

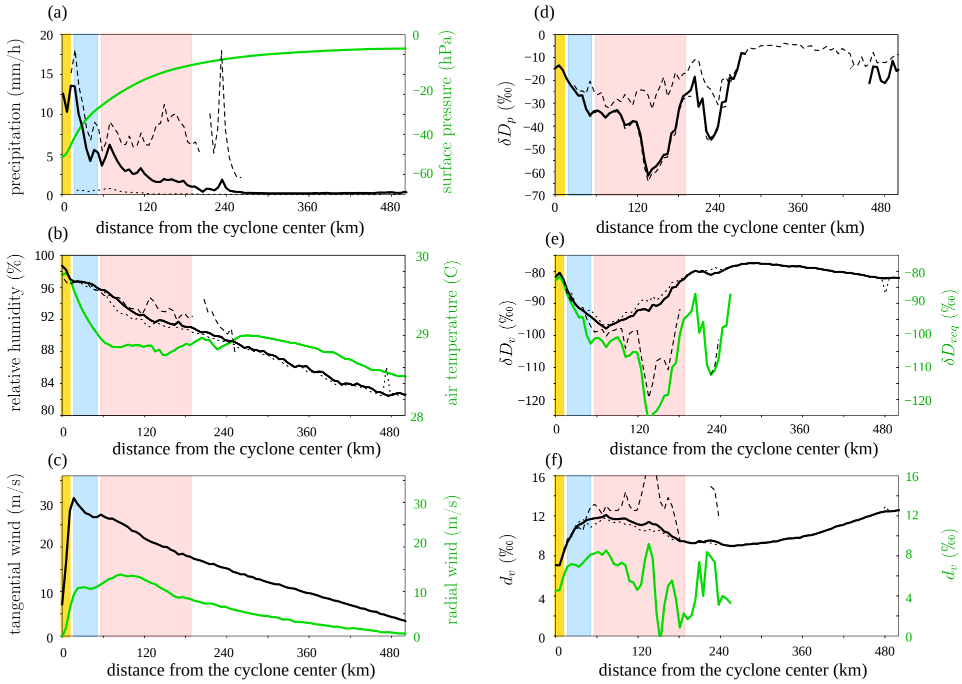

Figure 2. Evolution of surface variables as a function of distance to the storm center: Precipitation rate (a, black), surface pressure (a, green), near-surface air temperature (b, black), near-surface relative humidity (b, green), tangential (c, black) and radial (c, green) wind, surface precipitation δD (d), near-surface water vapor δD (e, black), water vapor δD that would be in equilibrium with the precipitation (e, green), near-surface water vapor d-excess (f, black) and precipitation d-excess (f, green). In d and e, dashed and dotted black lines indicate the same as black lines but for grid points where the precipitation rate is respectively higher and lower than 4 times the domain-mean precipitation, representing respectively the rain bands and in-between rain bands. The yellow, blue and pink rectangles indicate the eye, eyewall and rain band sub-domains respectively.

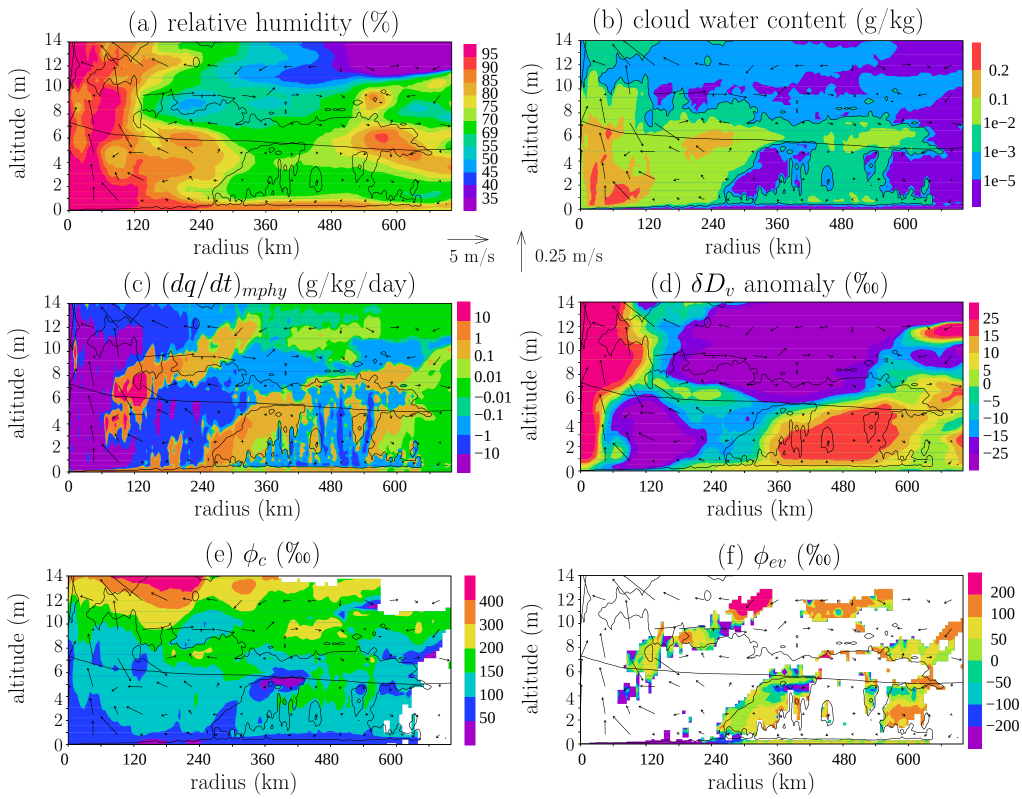

Figure 3. Variables as a function of altitude and of the distance r to the storm center: (a) Relative humidity; (b) cloud water content (cloud condensate and cloud ice); (c) specific humidity tendency due to phase changes (negative and positive values represent condensation and evaporation); (d) water vapor δD anomaly with respect to the domain-mean δD_v at each level; (e) relative enrichment $\phi_c = R_c/R_v$ of the isotopic ratio of the hydrometeors (cloud condensate, cloud ice, rain, graupel and snow) R_c relative to that in the vapor R_v; (f) relative enrichment of the isotopic ratio of the hydrometeor evaporation relative to the water vapor isotopic ratio $\phi_{ev} = R_{ev}/R_v$. The vectors show the radial and vertical components of the wind. The nearly-horizontal black line shows the 0°C isotherm. The black contours highlights the 10^{-3} g/kg contour for cloud water content.

depleted than if in equilibrium with the vapor. This suggests that the rain forms in altitude and undergoes little evaporative enrichment as it falls, consistent with the high relative humidity. In addition, it quickly falls to the ground without having the time to fully equilibrate isotopically with the vapor.

3.1.4 Qualitative comparison with isotopic observations

Observed isotopic patterns in tropical cyclones can be very diverse (Guilpart, 2018). However, some robust features emerge. The few studies that sampled water vapor or precipitation in the eye found that it was relatively enriched (Gedzelman et al., 2003; Fudeyasu et al., 2008). Outside the eye, many studies have observed that the water vapor and precipitation is more depleted towards the storm center (Gedzelman et al., 2003; Fudeyasu et al., 2008; Munksgaard et al., 2015; Jackisch et al., 2020; Skrzypek et al., 2019; Xu et al., 2019; Sanchez-Murillo et al., 2019). At a given distance from the storm center, the water vapor or precipitation is often more depleted in rain bands than in between (Munksgaard et al., 2015; Guilpart, 2018).

The observed d-excess in water vapor or precipitation is weaker in the eye (Fudeyasu et al., 2008), higher in the environment and higher in the rain bands than in-between (Munksgaard et al., 2015).

All these features are consistent with our simulation.

3.2 Squall line

3.2.1 Meso-scale structure

Figure 1 shows maps of precipitation rate, near-surface air temperature, surface pressure anomaly, near-surface relative humidity, near-surface water vapor δD and surface rain δD for an arbitrary snapshot. In presence of wind shear, the convection organizes into lines of intense precipitation perpendicular to the imposed surface winds (Figure 4a). The environment is very dry, with only a few isolated cumulonimbi. Under the squall line, a cold pool is driven by meso-scale downdrafts (Zipser, 1977; Gamache & Houze, 1981). The cold pool has a very sharp edge at the front of the line, corresponding to the gust front, and a long trail due to the imposed rearward horizontal winds near the surface (Figure 4b).

To better document the different parts of the squall line, we plot composites of meteorological and isotopic variables as a function of the along-x distance to the gust front (Figures 5 and 6). At each snapshot, for each row of the domain where the precipitation rate exceeds the domain-mean value, we select the x for which the along-x pressure gradient is maximum. If the pressure gradient exceeds 1.7 Pa/km, we assume that it is a gust front. This threshold was visually defined to optimally detect gust fronts. We define a new x-axis and translate all rows so that all gust fronts of the different rows are aligned at x_{gust}=30 km. We arbitrary set x_{gust}=30 km so that the squall lines stand in the middle of the composite plots. Rows of the domain where the precipitation is lower than the domain mean, or where a gust front could not be identified, are considered “environment” and are not taken into account in the composite.

The precipitation rate is maximum just after the gust front (Figure 5a), consistent with observations (Chong, 2009). The maximum precipitation locates where the along-x near-surface surface wind becomes null (Figure 5c), favoring the maintenance of strong updrafts (Rotunno et al., 1988). Elsewhere, the surface wind blows rearward. Near the gust front, the temperature drops and the relative humidity rises (Figure 5c). The recovery to their environment value is slow due to the rearward advection.

Our simulated squall line shows only one precipitation peak. This is at odds with observations that often show two peaks, one for the convective region and one for the stratiform region, separated by a transition region (Biggerstaff & Houze Jr, 1991; Chong, 2009). In our simulation, the convective region transitions continuously to the stratiform region. Increasing the horizontal resolution to 1 km did not help to simulate a transition region.

In spite of this shortcoming, the convective and stratiform regions of the squall line can be identified from water vapor tendencies (Figure 6b).The convective region can be identified by its intense condensation throughout the full troposphere (Figure 6b, around 50-60 km). The stratiform region can be identified by the condensation restricted to the upper troposphere (the anvil) and evaporation below (meso-scale downdraft) (Figure 6b, around 60-80 km). This pattern of condensation and evaporation is consistent with what we know from the squall line water budgets (Gamache & Houze, 1983; Chong & Hauser, 1990).

3.2.2 Definition of the sub-domains

Based on the above description of the meso-scale structure, we divide the grid points into 4 sub-domains.

Given the continuous transition in our simulations, we define the convective and stratiform sub-domains based on a precipitation threshold. For rows where x_{gust} is defined, we define:

- the convective region for x between x_{gust} and x_{xconv}, where x_{conv} is the first x values for which the precipitation comes back below 8 times the domain-average precipitation (yellow rectangle in Figure 5).
- the stratiform region for x between x_{conv} and x_{strati}, where x_{strati} is the first x values for which $x > x_{conv}$ and the precipitation is below the domain-average precipitation (blue rectangle in Figure 5).

The horizontal winds near the surface spread the cold pool rearward beyond the precipitating region. Therefore, we also define a sub-domain called "trailing", for x between x_{strati} and x_{trail} , where x_{trail} is the x value for which $x > x_{strati}$ and $T(x) < T(x_{gust})-1$, where T is the near-surface temperature in K (pink rectangle in Figure 5). All grid points that are not categorized as "convective", "stratiform" or "trailing" are called "environment" (left in white in Figure 5).

3.2.3 Simulated isotopic evolution

Simulated squall lines show a progressive depletion of the vapor in the convective region, maximum depletion at the end of the convective region, and a long recovery in the stratiform and trailing regions (Figure 5e). The δD_v reaches its environment value about 100 km after the convective peak.

The δD_p varies in concert with δD_v (Figure 5d). In the convective and stratiform regions, δD_p is more depleted than in equilibrium with the vapor (Figure 5e, red), consistent with a quick fall with little time to equilibrate and little evaporative enrichment. The weak precipitation that falls upwind of the convective region, where the air is dry, has a δD_p higher than that in equilibrium with vapor, indicating evaporative enrichment during rain evaporation.

D-excess is higher in the vapor in the convective, stratiform and trailing regions (Figure 5f). The low d-excess in the precipitation reflect the effect of evaporative enrichment, especially before the gust front and in the trailing region.

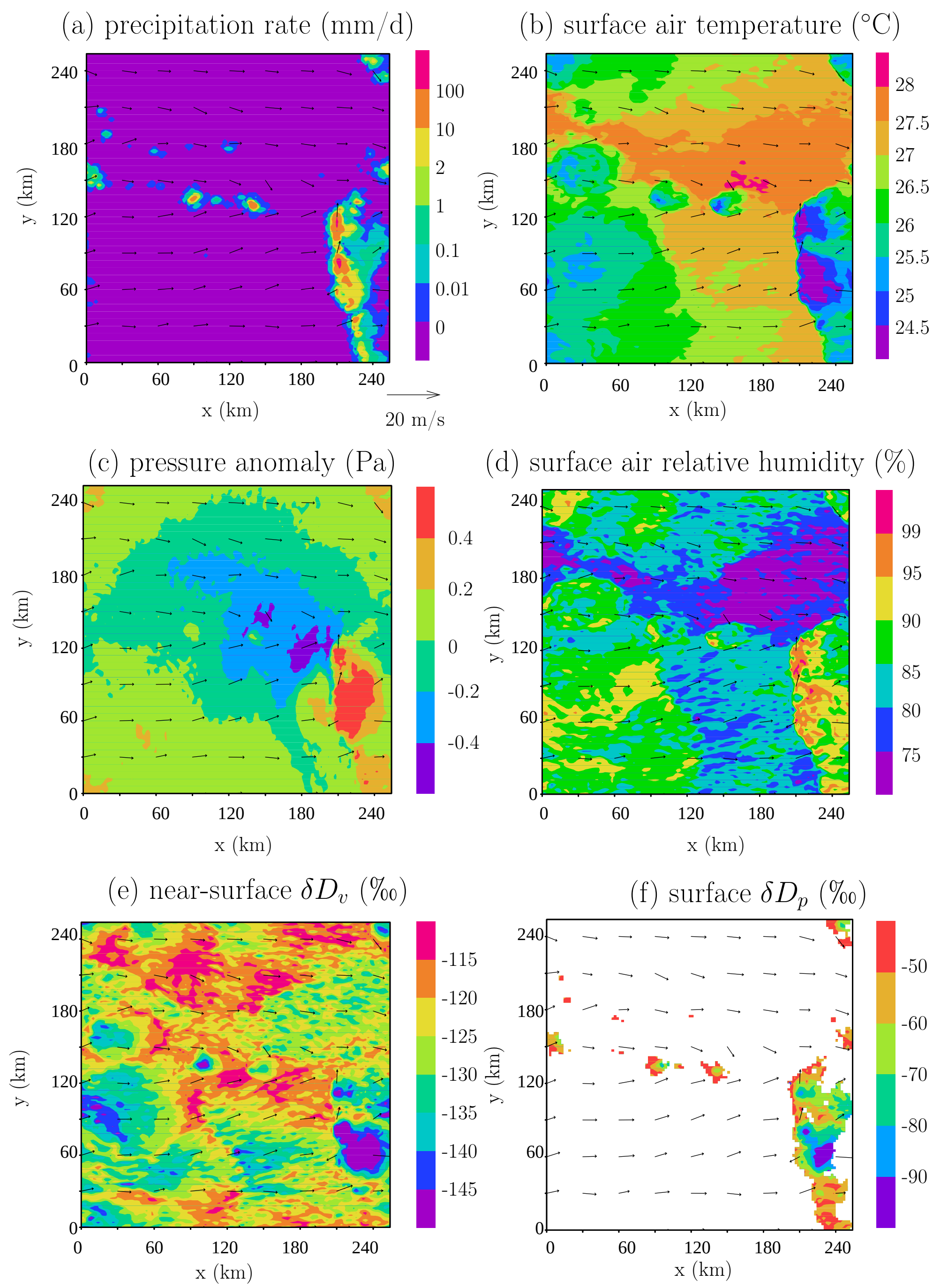

Figure 4. Same as Figure 1 but for the squall line. Note that due to the doubly periodic domain, the trailing region on the right edge of the domain continues on the left edge.

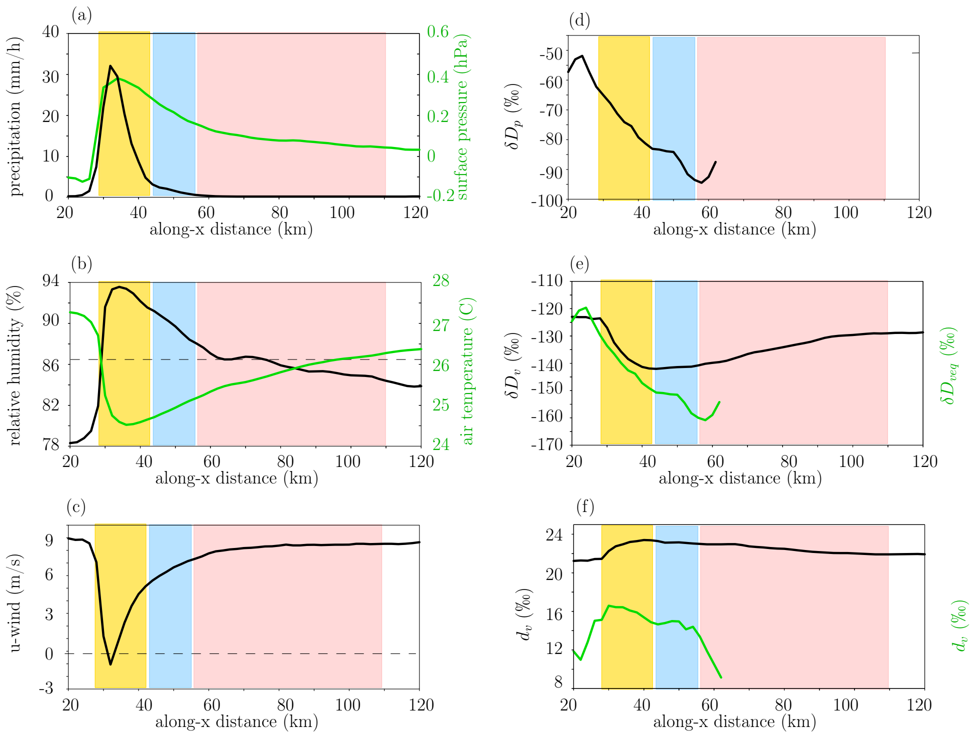

Figure 5. Evolution of surface variables as a function of distance along the x-axis, as a composite of all rows of all snapshots where a gust front could be defined (see text): Precipitation rate (a, black), surface pressure (a, green), near-surface air temperature (b, green), near-surface relative humidity (b, black), u-wind (c, black), surface precpitation δD (d), near-surface water vapor δD (e, black), water vapor δD that would be in equilibrium with the precipitation (e, green), near-surface water vapor d-excess (f, black) and precipitation d-excess (f, green).

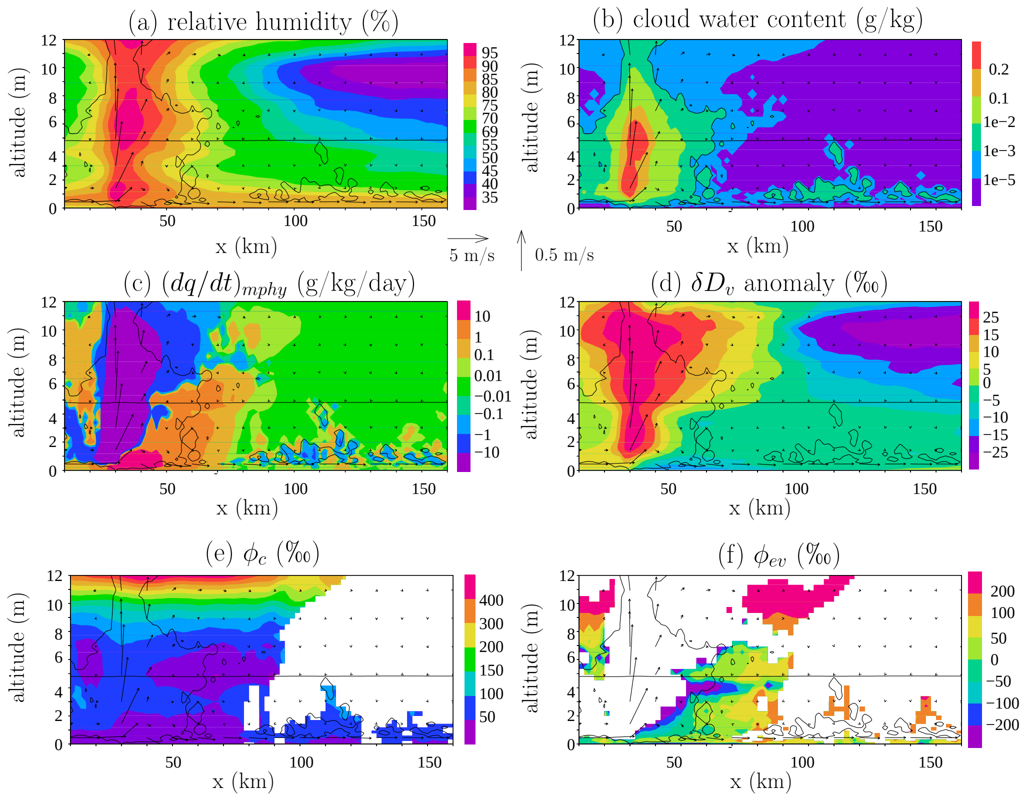

Figure 6. Relative humidity (a), specific humidity tendency due to phase changes (b; negative and positive values represent condensation and evaporation), water vapor δD anomaly (c) and the relative enrichment of the isotopic ratio of the hydrometeor evaporation relative to the water vapor isotopic ratio $\phi_{ev} = R_{ev}/R_v$ (d) as a function of altitude and of the distance along the x-axis. The vectors show the wind, with the vertical wind multiplied by 20 for better readability. The thick dashed horizontal black lines indicate the melting level.

3.2.4 Qualitative comparison with isotopic observations

Isotopic observations during squall lines often show a “W” shape with minimum δD_p in the convective and stratiform regions and a local maximum in the transition region (Taupin & Gallaire, 1998; Risi et al., 2010). Our simulation is consistent with this observation, except that since our simulation does not exhibit any transition region, it shows a “V” shape instead of a “W” shape.

In the vapor, inspection of a large number of squall lines in the Sahel showed that the isotopic evolution can be very diverse, but some robust features emerge (Tremoy et al., 2014).

- In 80% of 74 observed squall lines in (Tremoy et al., 2014), there is a depletion in the convective region compared to the environment before the squall line. This is consistent with our simulation.
- More than half of the observed squall lines show additional depletion in the stratiform region (Tremoy et al., 2014). This is also consistent with our simulation.
- For squall lines showing an isotopic depletion in the convective or stratiform region, the recovery from this depletion takes several hours after the end of the rain (Tremoy et al., 2014). Considering a propagation speed of about 20 m/s, this is consistent with the recovery distance of about 100 km in our simulation.
- In 78% of observed squall lines, the “W” shape often observed in the precipitation is not observed in the vapor (Tremoy et al., 2014). Our simulations are thus consistent with this majority of squall lines

Our simulated isotopic evolution during the squall line thus captures the features that are most commonly observed in squall lines.

Some squall lines may feature very different variations, and even enrichment in the convective and stratiform regions (Tremoy et al., 2014). To check whether we could capture such a diversity of isotopic variations, we performed many sensitivity tests, including simulations without large-scale ascent, with large-scale ascent peaking in the upper troposphere to favor stratiform development (Su et al., 2000), increased horizontal resolution, interactive radiation, reduced sublimation or reduced rain evaporation to favor the maintenance of the stratiform region (Yang & Houze Jr, 1995; Bryan & Morrison, 2012), bowling alley domain, or prescribed horizontal wind in the upper troposphere to favor the development of the stratiform region (Caniaux et al., 1994). Depending on the simulations, the stratiform region is more or less extended and the squall lines are more or less organized, but the meteorological and isotopic evolution is always very similar. We thus keep in mind that our simulations are relevant for the majority of squall lines, but not all of them. In addition, some features in some of the squall line observed over land might not be captured by our simulations with an oceanic setting.

4 Understanding mesoscale isotopic variations

4.1 Importance of rain evaporation

Observational and modeling studies highlighted the key role of rain evaporation and rain-vapor exchanges in depleting the water vapor within organized systems (Lawrence et al., 2004; Tremoy et al., 2014; Xu et al., 2019). In both the cyclone and the squall line, very dry air in the environment favor thick layers of rain evaporation in the free troposphere (Figure 3a,c, 6a,c).

In the simulated cyclone, they correspond to the two thick orange diagonals in Figure 3b. We notice that the δD pattern also shows a diagonal pattern of negative anomalies, descending inward and downward (Figure 3d), creating the depletion simulated near the surface in the eyewall and rain bands. For δD, the diagonal pattern is however much smoother. This suggests that rain evaporation favors the isotopic depletion of water vapor, which accumulates as air moves inward.

Similarly, in the squall line, strong evaporation occurs in the stratiform region, between 60 and 80 km (Figure 6b). Maximum evaporation occurs in the cold pool under the convective and stratiform region and coincides with the maximum depletion (Figure 6c).

To analyze the isotopic effect of rain evaporation in more detail, we calculate $\phi_{ev} = R_{ev}/R_v$, where R_v and R_{ev} are the isotopic ratio in water vapor and in hydrometeor evaporation. ϕ_{ev} represents the enrichment of rain evaporation relative to water vapor: if $(\phi_{ev} - 1) \cdot 1000 > 0‰$, rain evaporation enriches the water vapor; if $(\phi_{ev} - 1) \cdot 1000 < 0‰$, rain evaporation depletes the water vapor. R_{ev} is calculated as $(dq_{HDO}/dt)_{mphy}/(dq/dt)_{mphy}$, where q_{HDO} is the mixing ratio for HDO, q is the water vapor mixing ratio, and $(dq/dt)_{mphy}$ and $(dq_{HDO}/dt)_{mphy}$ are the water vapor and HDO tendencies associated with phase changes. The $(dq/dt)_{mphy}$ tendency is positive if dominated by rain or cloud water evaporation or sublimation of ice, snow or graupel, and negative if dominated by cloud condensation or deposition onto snow, cloud ice or graupel. R_{ev} is calculated only where $(dq/dt)_{mphy} > 0$.

We can see that near the rain bands of the cyclone and in the stratiform region of the squall line, there is a strongly depleting effect of rain evaporation just below the melting level (Figure 3f,6f). This is because just below the melting level, most of the rain originates from snow melt, which is very depleted (Figure 3e,6e) because it has formed high in altitude (Risi et al., 2021). The depleting effect of rain evaporation and diffusive exchanges in stratiform regions of convective systems has already been highlighted in previous studies (Kurita, 2013; Aggarwal et al., 2016), including in cyclones (Munksgaard et al., 2015).

There is also a depleting effect directly in the sub-cloud layer of the cyclone, probably because intense rain falls so fast and the air is so moist that diffusive exchange between the depleted rain and the vapor dominate and deplete the water vapor (Lawrence et al., 2004).

Elsewhere, rain evaporation has an enriching effect, especially where the air is dry and the rain rate is small (Tremoy et al., 2014). In the limit case where rain drops evaporate totally, $\phi_{ev} = R_p/R_v$ which is close to the fractionation coefficient α_{eq}. This is reflected by the orange shades at the periphery of the cyclone and in the trailing region of the squall line.

4.2 Simulations with de-activated fractionation during rain evaporation

One way to quantify the effect of rain evaporation and rain-vapor diffusive exchanges is to run additional simulations in which they are de-activated (Field et al., 2010; Risi et al., 2021). The simulations are the same for meteorological variables, but the rain-vapor diffusive exchanges are suppressed and the rain evaporation is assumed not to fractionate.

Without fractionation during rain evaporation, the mesoscale δD_v variations are strongly reduced (Figure 7). In cyclones, in absence of fractionation during rain-vapor interactions, the δD_v would be almost flat, and the maximum depletion would be in the environment (Figure 7a), contrary to observations and to the full simulations. In squall lines, the difference between the δD_v in the stratiform region and in the environment is reduced by 80%, and the δD_v recovers much more quickly after the squall line (Figure 7b).

This confirms the key role of rain evaporation and rain-vapor diffusive exchanges to deplete the low-level water vapor at the mesoscale scale.

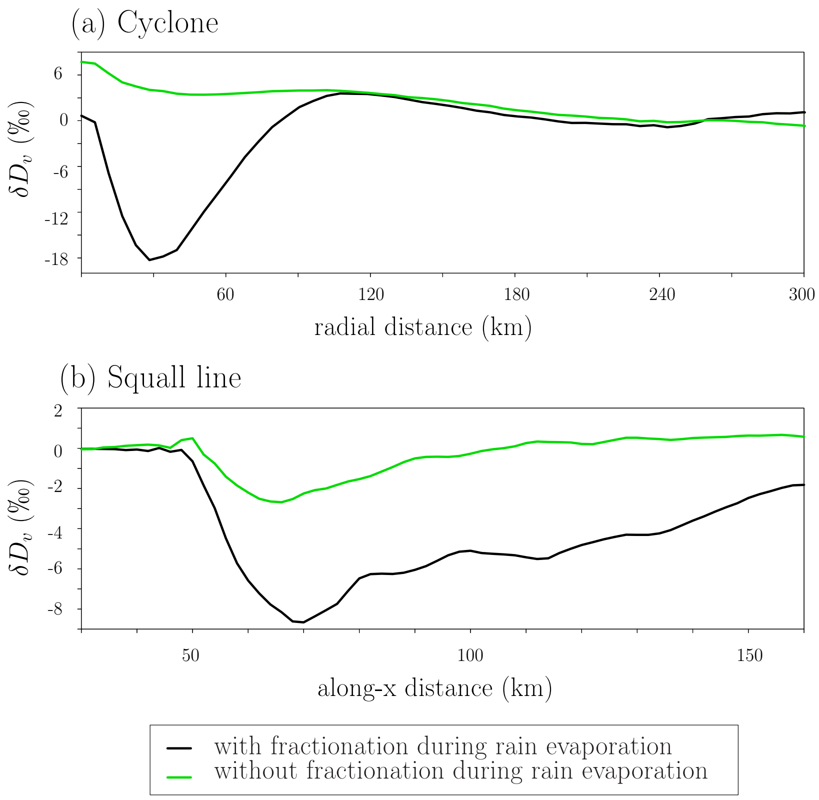

Figure 7. Evolution of near-surface δD_v as a function of r for tropical cyclones (a) and as a function of x for squall lines (b), in simulations in which rain evaporation and rain-vapor diffusive exchanges are activated (black) and de-activated (green).

4.3 Decomposition method

To quantify the relative importance of processes in determining the isotopic composition in the different parts of the domain, we design a simple box model for the subcloud layer (SCL) inspired from (Risi et al., 2020) (Figure 8a). The main difference is that here we account for horizontal advection and non-stationary effects, because the simple model will be applied in the different sub-domains of the simulation domains. Whereas the SCL is in quasi-equilibrium in the domain-mean, it is not in quasi-equilibrium in subdomains. For example, the eye of the cyclone wanders across the domain and is thus never in quasi-equilibrium.

The SCL is defined as the first atmospheric levels where the domain-mean cloud fraction remains below 10% of its maximum value. The water budget of the SCL in a given sub-domain writes (Figure 8a):

$$\frac{dW}{dt} = E_{sfc} + F_d(q_d - q) - F_u(q_u - q) + E_{horiz} + E_{ev} - E_c$$

where W is the water mass in the SCL per area unit (in kg/m2), E_{sfc} is surface evaporation, F_d and F_u are the downward and upward mass fluxes at SCL top, E_{horiz} is the flux of water through horizontal advection, E_{ev} is the rain evaporation, E_c is some condensation that may occur if the SCL top is not horizontally uniform, q_u and q_d are the specific humidity in updrafts and downdrafts and q is the specific humidity near the surface. All these variables can directly be diagnosed from the simulations for each subdomains.

Similarly, the isotopic budget writes:

$$\frac{d(R \cdot W)}{dt} = R_{sfc} \cdot E_{sfc} + F_d(R_d \cdot q_d - R \cdot q) - F_u(q_u - R \cdot q) + R_{horiz} \cdot E_{horiz} + R_{ev} \cdot E_{ev} - R_c \cdot E_c$$

where R is the isotopic ratio of the near-surface vapor, R_u and R_d are the isotopic ratios in updrafts and downdrafts, R_{sfc}, R_{horiz}, R_{ev} and R_c are the isotopic compositions of the surface evaporation, horizontal advection, rain evaporation and condensation fluxes.

We define:

$$E_{res} = E_{horiz} - \frac{dW}{dt}$$

It is the flux of water through both horizontal advection and non-stationary effects, and is calculated as a residual. For example, in the cyclone's eyewall where the air is very moist, we expect that horizontal advection will have a drying effect, i.e. $E_{horiz} < 0$. In addition, since the cyclone wanders across the domain, the eyewall often arrives in dry parts of the domain, i.e. $\frac{dW}{dt} > 0$. Therefore, both horizontal advection and non-stationary effects contribute to drying the eyewall, i.e. $E_{res} < 0$.

Similarly, we define the isotopic ratio of the flux R_{res}:

$$R_{res} = \frac{R_{horiz} \cdot E_{horiz} - \frac{d(R \cdot W)}{dt}}{E_{horiz} - \frac{dW}{dt}}$$

To solve the isotopic budget equation for R, the isotopic ratios R_{sfc}, R_d, R_u, R_{res}, R_{ev} and R_c are all expressed as a function of R. The isotopic ratio of surface evaporation is given by (Craig & Gordon, 1965):

$$R_{sfc} = \frac{R_{oce}/\alpha_{eq}(SST)}{\alpha_K \cdot (1-h)}$$

where R_{oce} is the isotopic ratio at the ocean surface, $\alpha_{eq}(SST)$ is the equilibrium fractionation coefficient at the sea surface temperature, α_K is kinetic fractionation coefficient (Merlivat & Jouzel, 1979) and h is the relative humidity normalized at the SST and accounting for ocean salinity: $h = q/q_{sat}^{surf}(SST)$, $q_{sat}^{surf}(SST) = 0.98 \cdot q_{sat}(SST)$ and q_{sat} is the humidity saturation as a function of temperature at the sea level pressure. We assume $\delta D_{oce} = 0‰$ and h is diagnosed from the CRM. The kinetic fractionation is a function of surface wind speed and is also diagnosed from the CRM.

The isotopic ratios in updrafts and downdrafts are assumed to follow logarithmic functions: $R_u = R \cdot \left(\frac{q_u}{q}\right)^{\alpha_u - 1}$ and $R_d = R \cdot \left(\frac{q_d}{q}\right)^{\alpha_d - 1}$ where R_u and R_d are isotopic ratios in updrafts and downdrafts, and α_u and α_d are the $q{-}\delta D_v$ steepness coefficients for updrafts and downdrafts (Risi et al., 2020). We set $R_{res} = \phi_{res} \cdot R$, $R_{ev} = \phi_{ev} \cdot R$ and $R_c = \phi_c \cdot R$. All parameters α_u, α_d, ϕ_{res}, ϕ_{ev} and ϕ_c can be diagnosed from the simulation for each sub-domain.

We get:

$$R = \frac{R_{oce}/\alpha_{eq}(SST)}{h + \alpha_K \cdot (1-h) \cdot A} \tag{1}$$

where

$$A = \frac{((q_u/q)^{\alpha_u} - 1) + \frac{F_d}{F_u} \cdot (1 - (q_d/q)^{\alpha_d}) - \frac{E_{ev}}{qF_u} \cdot \phi_{ev} + \frac{E_c}{qF_u} \cdot \phi_c - \frac{E_{res}}{qF_u} \cdot \phi_{res}}{(q_u/q - 1) + \frac{F_d}{F_u} \cdot (1 - q_d/q) - \frac{E_{ev}}{qF_u} + \frac{E_c}{qF_u} - \frac{E_{res}}{qF_u}} \tag{2}$$

Note that the diagnostic of E_{res} and ϕ_{res} as residuals guarantees that the water and isotopic budgets of the SCL are closed. However, it does not guarantee that equation 1 with input parameters diagnosed from the CRM simulations yields exactly the same isotopic ratios as those directly simulated by the CRM, because of the numerous simplifying assumptions underlying the simple model.

In each sub-domain of a simulation, we calculate R from equation 1 in 8 different ways, de-activating different effects one by one (table 1). By calculating the differences between these different simulations, we can decompose R into 7 contributions. We explain below how these contributions are calculated, with names of calculations defined in table 1. We also explain the physical meaning of these contributions, which is illustrated in Figure 8b:

1. Mean_wind-Mean_h represents the effect of near-surface relative humidity (Figure 8b, red). Near-surface relative humidity impacts the kinetic processes during ocean surface evaporation (Merlivat & Jouzel, 1979).
2. Merlivat-Mean_wind represents the variations in the kinetic fractionation coefficient α_K, which are mainly due to variations in surface wind speed (Merlivat & Jouzel, 1979) (Figure 8b, orange).
3. No_grad-Merlivat represents the effect of the horizontal humidity contrasts (Figure 8b, green). When horizontal humidity contrasts between dry and moist zones of a sub-domain are larger, dry subisent regions import drier air and more depleted water vapor in the SCL, while ascending regions export moister air and more enriched water vapor in the SCL. This has thus a depleting effect.
4. No_ev-No_grads represents the effect of variations in the steepness of the relationship between q and δD_v for updrafts and downdrafts. When the $q{-}\delta D_v$ steepness is larger, downdrafts import more depleted vapor into the SCL and updrafts

export more enriched vapor out of the SCL (Risi et al., 2021). The $q-\delta D_v$ steepness depends on the enriching or depleting processes that occur above the SCL. Typically, the dominant effect is rain evaporation above the SCL, which depletes the water vapor, especially near the melting level (Risi et al., 2021) (Figure 8b, blue). Herafter for simplicity, we will call this contribution "Rain evaporation above the SCL" because this is the main process underlying this contribution. But we keep in mind that it might encompass in reality a wider range of processes (e.g. entrainment in cloud updrafts (Risi et al., 2021)).

5. No_cond-No_ev represents the effect of rain evaporation in the SCL (Figure 8b, purple).
6. No_adv-No_cond represents the effect of condensation in the SCL (Figure 8b, cyan).
7. Full-No_adv represents horizontal advection and non-stationary effects (Figure 8b, brown).

By construction, the sum of these 7 contributions yields Full-Mean_h, which corresponds to the sub-domain-mean anomaly relative to the domain-mean.

4.4 Water budget in each sub-domain

4.4.1 Cyclone

The cyclone in itself (sub-domains 1-4) covers less than 1% of the domain (Figure 9a). In all sub-domains, the main source of water vapor is surface evaporation (Figure 9b red). It is more than twice larger in the eyewall, in rain bands and in-between rain bands than in the environment, consistent with the maximum winds, and less than half in the eye, due to weak winds and very moist near-surface air. Rain evaporation is also a significant moistening term in the eyewall and in the rain bands (pink). Condensation is insignificant (Figure 9b cyan). Everywhere except in the eye, updrafts and downdrafts have a drying effect (green and blue), because updrafts are preferentially moister and downdrafts are preferentially drier. In the eye, updrafts and downdrafts slightly moisten the SCL because the core of the eye is descending and almost saturated whereas air parcels near the eyewall may be drier and ascending. Horizontal advection and non-stationary effects dry the cyclone and slightly moisten the environment (brown). This is because dry air from the environment converge towards to cyclone center (horizontal advection effect). In addition, the cyclone wanders across the domain and thus mixes with air that was previously in the dry portions of the domain (non-stationary effect). In turn, in the wake of the cyclone, the environment is left moistened.

4.4.2 Squall line

The squall line and its trailing region (sub-domains 1-3) cover about 15% of the domain (Figure 10a). Surface evaporation is the main source of water in the SCL and is approximately uniform in all sub-domains (Figure 10b red). The rain evaporation is a significant source in both the convective and stratiform parts (pink). In the convective part, the main sink of water is the export of moist air through updrafts (green), consistent with the very vigorous updrafts. Horizontal advection and non-stationary effects moisten the convective zone by advecting air from the stratiform region moistened by rain evaporation, and dries the trailing region by advecting drier air from the environment (brown).

4.5 Decomposition of the isotopic composition in each sub-domain

4.5.1 Cyclone

Regarding δD_v, the simple model is able to capture the main isotopic differences between the different sub-domains, especially the relatively more enriched eye, the max-

Table 1. Different calculations of the isotope ratio following equations 1 and 2, allowing us to de-activate different effects one by one. For each calculation, we give the values of different input parameters (columns 2 to 10). "sub" means that we use the values diagnosed from the CRM for each sub-domain. $\bar{\alpha_z}$ is the average $q - \delta D_v$ steepness over the full domain (Risi et al., 2021). The "Merlivat" calculation is identical to the traditional (Merlivat & Jouzel, 1979) closure. The "Full" calculation corresponds to the calculation with all 7 contributions included. In contrast, the "Mean_h" calculation includes none of the 7 contributions, and yields the same results for all sub-domains. The 7 contributions to the SCL water vapor isotopic ratio are then calculated by differences between these different calculations (last column).

Name of the calculation	h	α_K	q_u	q_d	α_u	α_d	E_{ev}	E_c	ϕ_{res}	Effect that it allows to isolate
Mean_h	domain-mean h	domain-mean α_K	q	q	$\bar{\alpha_z}$	$\bar{\alpha_z}$	0	0	1	Constant reference
Mean_wind	sub	domain-mean α_K	q	q	$\bar{\alpha_z}$	$\bar{\alpha_z}$	0	0	1	Mean_wind-Mean_h = near-surface relative humidity (#1)
Merlivat	sub	sub	q	q	$\bar{\alpha_z}$	$\bar{\alpha_z}$	0	0	1	Merlivat-Mean_wind = surface wind speed (#2)
No_grad	sub	sub	sub	sub	$\bar{\alpha_z}$	$\bar{\alpha_z}$	0	0	1	No_grad-Merlivat = horizontal humidity contrasts (#3)
No_ev	sub	sub	sub	sub	sub	sub	0	0	1	No_ev-No_grads = rain evaporation above the SCL (#4)
No_cond	sub	sub	sub	sub	sub	sub	sub	0	1	No_cond-No_ev = rain evaporation in the SCL (#5)
No_adv	sub	sub	sub	sub	sub	sub	sub	sub	1	No_adv-No_cond = condensation in the SCL (#6)
Full	sub	sub	sub	sub	sub	sub	sub	sub	sub	Full-No_adv = horizontal advection and non-stationary effects (#7)

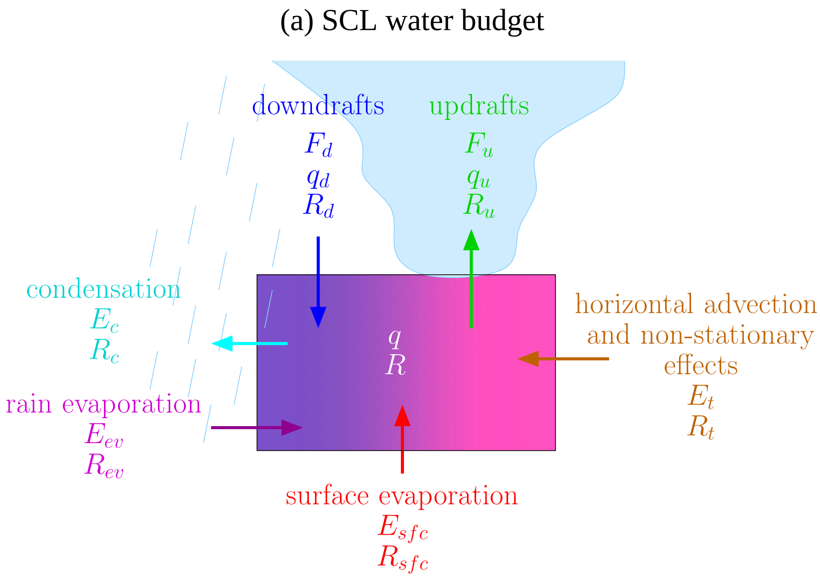

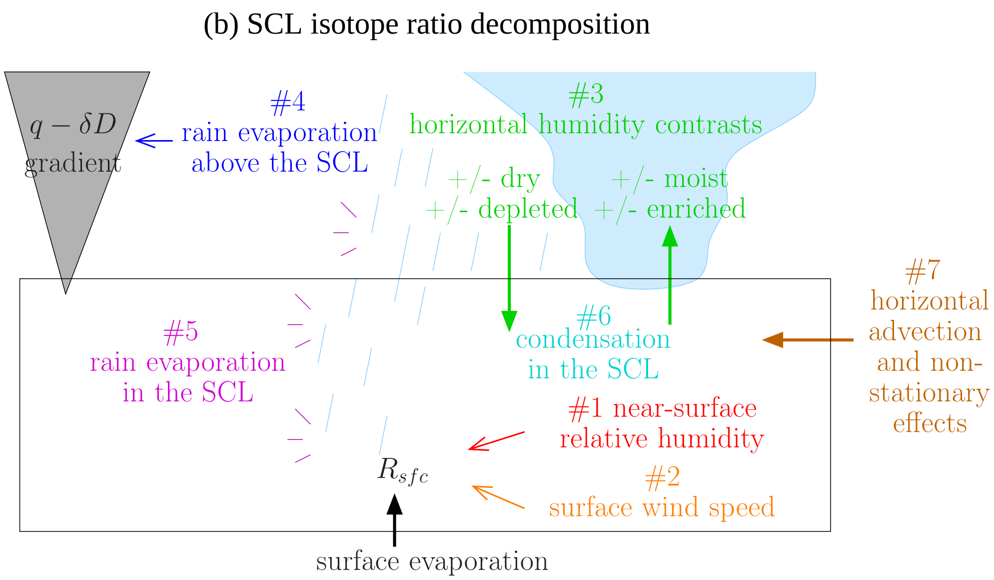

Figure 8. (a) Simple model to predict the SCL water vapor composition. It accounts for surface evaporation, rain evaporation, cloud condensation, updrafts and downdrafts at the SCL top, and horizontal advection and non-stationary effects quantified as a water budget residual. (b) Schematic illustrating the 7 contributions in the decomposition of the isotopic ratio: near-surface relative humidity (#1, red) and surface wind speed (#2, orange), which both contribute to control the isotope composition of the surface evaporation; horizontal humidity contrasts (#3, red) and rain evaporation above the SCL (#4, blue), which both contribute to the SCL depletion by vertical mixing; rain evaporation (#5, purple) and condensation (#6, cyan) within the SCL; and horizontal and non-stationary effects (#7, brown).

imum depletion in the eyewall, the relatively depleted rain bands and the relatively enriched environment (Figure 9c).

Rain evaporation and rain-vapor diffusive exchanges in the SCL (Figure 9d pink) are the main drivers of the depletion in the rain bands and in the eyewall. Alone, it would deplete the rain bands and the eyewall relative to the environment by about 7‰ and 28‰, greater than the total predicted depletion relative to the environment. This is due to the very depleted isotopic signature of rain evaporation in the SCL (Figure 3d), and this is consistent with the strong contribution of isotopic fractionation to rain evaporation (section 4.2).

The rain evaporation above the SCL (Figure 9d blue) also contributes to deplete the rain bands and in the eyewall relative to the environment, by about 9‰. This effect is consistent with the very depleted isotopic signature of rain evaporation near the melting level (Figure 3d), and also contributes to the strong contribution of isotopic fractionation to rain evaporation estimated (section 4.2).

These two effects are partially counter-balanced by the stronger humidity contrast (Figure 9d green) in the environment, reflecting drier and more depleted conditions in the mid-troposphere associated with the compensating subsidence in the environment.

Horizontal advection and non-stationary effects (Figure 9d brown) have a smoothing effect on the isotopic patterns mainly driven by rain evaporation. In particular between rain bands, they are the main depleting factor, contributing to a 10‰ depletion relative to the domain-mean. This is because horizontal winds bring depleted water vapor from the rain bands (Figure 9d). In the eyewall, horizontal advection and non-stationary effects contribute to a 2‰ depletion relative to the domain-mean, because horizontal winds bring depleted water vapor from rain bands. Horizontal advection has an enriching effect in rain bands, where the isotopic gradients are reversed: horizontal winds bring enriched water vapor from in-between rain bands.

The other contributions, including the effects of relative humidity and kinetic fractionation during surface evaporation and of condensation in the SCL, have a marginal impact on δD_v. The marginal impact of condensation is consistent with the absence of clouds in the SCL, and confirms that rain-out does not directly impact the SCL isotopic composition.

A relative enrichment inside the eye is simulated in spite of the neglect of sea spray in our simulations. In our simulation, this enrichment is explained by the weak rain evaporation and by the relatively weak horizontal advection into the eye (Figure 9b). Therefore, the simple model simulates an isotopic composition that is similar to that predicted by (Merlivat & Jouzel, 1979). This does not exclude the possibility for a role of sea spray in nature (Fudeyasu et al., 2008), but this role is not necessary to explain the enrichment in the eye.

Regarding d-excess, the simple model captures the maximum d_v in the rain bands (Figure 9e). This is mainly due to the rain evaporation in the SCL (Figure 9f, purple), which yields water vapor with very high d-excess because of the relatively larger diffusivity of HDO relative to that of $H_2^{18}O$. Alone, it would contribute to an increase in d-excess by more than 7‰ relative to the environment, i.e. more than 150% of the total d-excess difference. Rain evaporation also acts to increase d-excess in the eyewall.

The stronger winds, resulting in stronger kinetic fractionation during surface evaporation, also play a significant role (Figure 9f, orange). It increases the d-excess by about 2‰ in the eyewall, bands and in-between bands, relative to the environment.

The simple model also captures the weakest d_v values in the eye (Figure 9e). These weak values are due to the moist conditions in the eye that reduce the kinetic effects during surface evaporation (Figure 9f, red).

As for δD_v, horizontal advection acts to smooth the d-excess patterns (Figure 9f, brown).

To summarize, the δD_v differences between the sub-domains are mainly explained by rain evaporation and rain-vapor diffusive exchanges inside the SCL, which deplete the eyewall and rain bands, consistent with previous studies (Gedzelman et al., 2003). The d-excess differences between the sub-domains are explained both by rain evaporation and by kinetic effects during surface evaporation. Horizontal advection plays a key role to smooth the isotopic patterns, contributing to the progressive depletion as the air converges towards the center of cyclones suggested in previous studies (Gedzelman et al., 2003; Xu et al., 2019).

4.5.2 Squall line

The simple model captures the maximum depletion in the stratiform region and the depletion in the convective and trailing regions (Figure 10c).

In both the convective and stratiform parts of the squall line, two terms mainly contribute to the depletion:

1. rain evaporation and rain-vapor diffusive exchanges in the SCL deplete the water vapor (Figure 10d, purple). Alone, it would deplete the convective and stratiform regions by about -100 and -50 ‰ respectively, far exceeding the total difference relative to the environment.
2. Rain evaporation above the SCL also contributes to the depletion (Figure 10d, blue).

These two processes are consistent with the depleting effect of rain evaporation both in the SCL and near the melting level (Figure 6d), and with the major effect of fractionation during rain evaporation on the isotopic evolution in squall lines (section 4.2).

In the convective region, the humidity contrast (Figure 10d, green) also contributes to the depletion relative to the environment. This may be due to the fact that the convective region is near the environment boundary, and thus experiences strong horizontal humidity gradients.

In the trailing region, where the precipitation is very small, the depletion is explained by horizontal advection and non-stationary effects (Figure 10d, brown). Alone, it would contribute to a 40‰ depletion relative to the domain mean. This reflects the effect of horizontal advection spreading the depleted water vapor from the stratiform region. The environment is similarly, but to a lesser extent, affected by this depleting effect of rearward horizontal advection. In contrast, the horizontal advection explains why the convective region is less depleted than the stratiform region: horizontal advection brings enriched water vapor from the environment towards squall line front.

Regarding d-excess, the slightly higher d_v in the stratiform region is mainly explained by rain evaporation both within and above the SCL (Figure 10d, purple and blue). Rain evaporation in the SCL strongly increases d_v in the convective region (Figure 10d, purple), but this is compensated by the advection of vapor from the environment with a lower d_v (Figure 10d, brown).

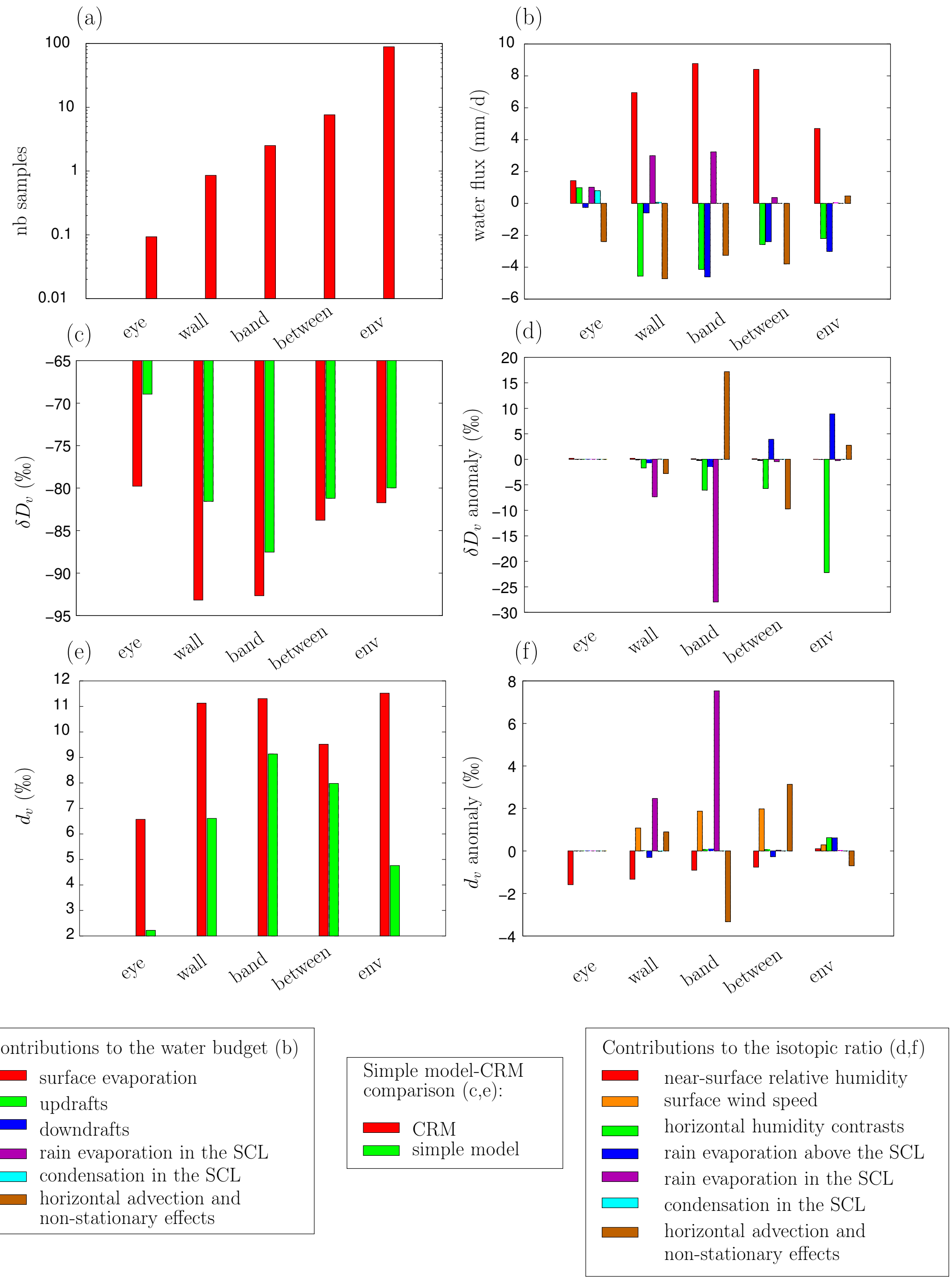

Figure 9. (a) fraction of the domain covered by the five sub-domains of the cylone: eye, eyewall ("wall"), rain bands ("bands"), in-between bands ("between") and the environment ("env"). (b) Water fluxes contributing to the water budgets of the different sub-domains of the cyclone: Surface evaporation (red), updrafts (green), downdrafts (blue), rain evaporation (pink), condensation (cyan) and residual term associated with horizontal advection and non-stationary effects (yellow). (c) δD_v simulated by SAM (red) and by the simple model (green). (d) Decomposition of the δD_v difference between the sub-domain and the domain-mean into 7 contributions: near-surface relative-humidity (red), surface wind speed (orange), horizontal humidity contrasts (green), rain evaporation above the SCL (blue), rain evaporation within the SCL (purple), condensation within the SCL (cyan) and horizontal advection and non-stationary effects (brown). (e-f) Same as (c-d) but for d_v.

Variations in near-surface relative humidity and winds are smaller than in the cyclone simulations, so the contributions of these effects are marginal.

To summarize, the δD_v differences between the sub-domains are explained by rain evaporation and rain-vapor diffusive exchanges inside the SCL, and also probably above the SCL. This is consistent with previous studies (Risi et al., 2010; Tremoy et al., 2014). Horizontal advection then plays a key role in spreading the isotopic anomaly rearward.

4.5.3 Discussion

We find many common aspects for the mesoscale isotopic variability between cyclone and squall line simulations.

- In both cases, rain evaporation and rain-vapor diffusive exchanges both within and above the SCL (especially near the melting level) are the main drivers of isotopic depletion in the most depleted parts of the convective systems (eyewall and rain bands for the cyclone, convective and stratiform parts of the squall line). This is consistent with previous studies (Gedzelman et al., 2003; Tremoy et al., 2014; Xu et al., 2019). These processes have also a crucial impact on d-excess.
- In both cases, horizontal advection and non-stationary effects act to smooth the isotopic patterns. It leads to the gradual depletion towards the eyewall observed in tropical cyclones, and it spreads the isotopic anomalies rearward in the case of the squall line. This is consistent with previous studies (Xu et al., 2019).
- In both cases, condensation processes have no direct effect on the SCL water vapor. It only has an indirect effect through maintaining a vertical gradient in δD_v that allows the rain evaporation to have a depleting effect on the SCL water vapor. In tropical cyclones for example, the rain-out along trajectories has been suggested in some studies to explain the progressive depletion towards the eyewall. We saw here that this is not the case.

The main difference between the two simulations is in the effect of kinetic effects during surface evaporation. Strong winds and very moist conditions in tropical cyclones significantly impact the d-excess, whereas they have a marginal effect in squall lines.

5 Conclusion

Using cloud resolving model simulations of cyclones and squall lines, and a simple SCL budget model, we investigate how convective processes impact the isotopic composition of water vapor and precipitation at the meso-scale. Figure 11 summarizes our results. We show that the main factors depleting the water vapor at the meso-scale is rain evaporation, especially in the sub-cloud layer of rain bands and of the eyewall in tropical cyclones, and in the meso-scale downdraft of the stratiform region in squall lines. The meso-scale δD_v patterns are subsequently reshaped by horizontal advection. These mechanisms are overall consistent with those suggested in previous studies (Gedzelman et al., 2003; Tremoy et al., 2014; Xu et al., 2019). In contrast to previous studies however, we highlight that condensation has no direct impact and that the evaporation of sea spray is not necessary to explain the relative enrichment in the cyclone eye.

This study strengthens our understanding of mesoscale isotopic variability. It provides physical arguments for the more depleted rain in tropical cyclones or squall lines relative to the rain in their environment. Therefore, this study supports the interpretation of paleoclimate isotopic archives in tropical regions in terms of past cyclonic activity (Nott et al., 2007; Medina-Elizalde & Rohling, 2012; Baldini et al., 2016) or past

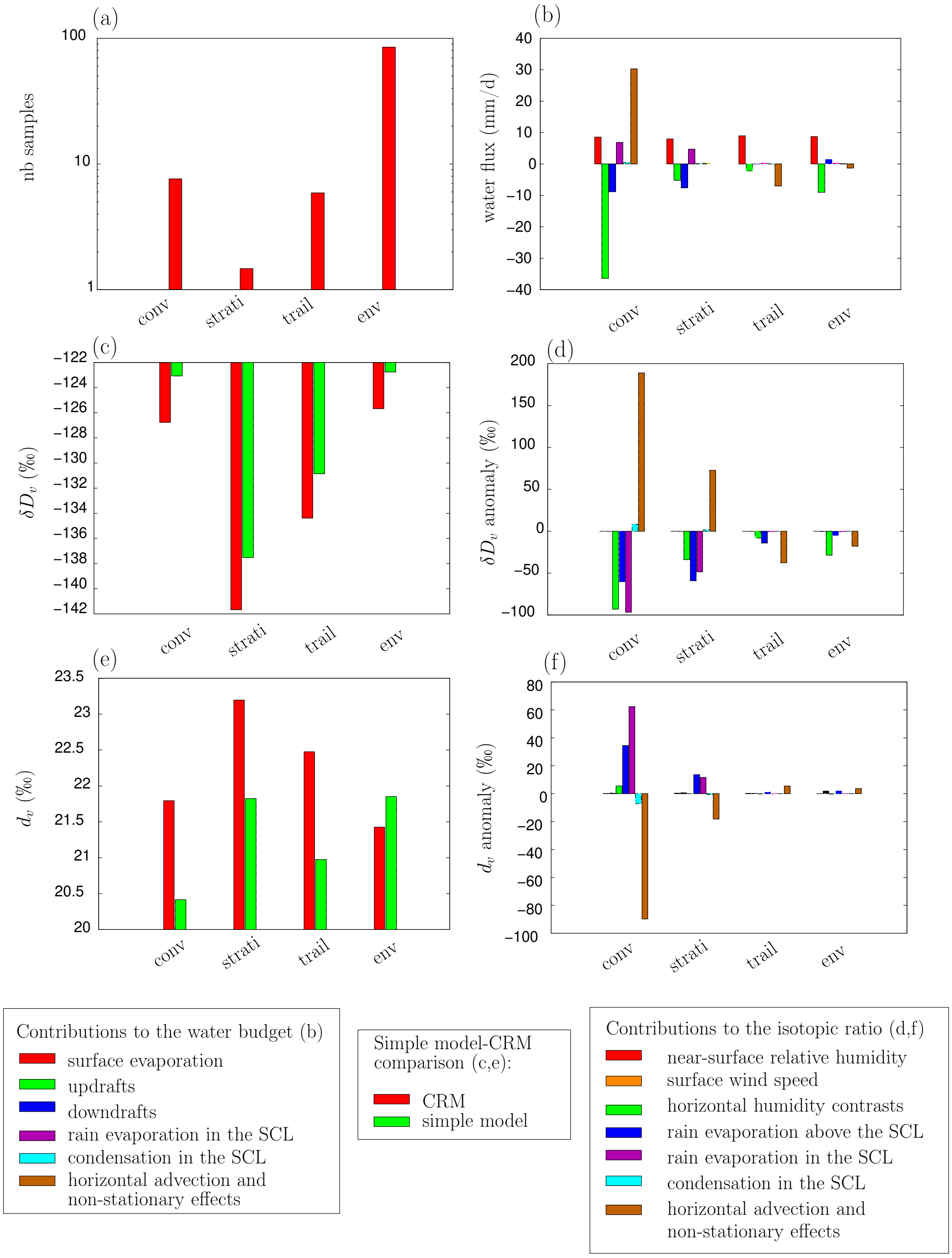

Figure 10. Same as Figure 9 but for the four sub-domains of the squall line: convective ("conv"), stratiform ("strati") and trailing ("trail") regions, and the environment ("env").

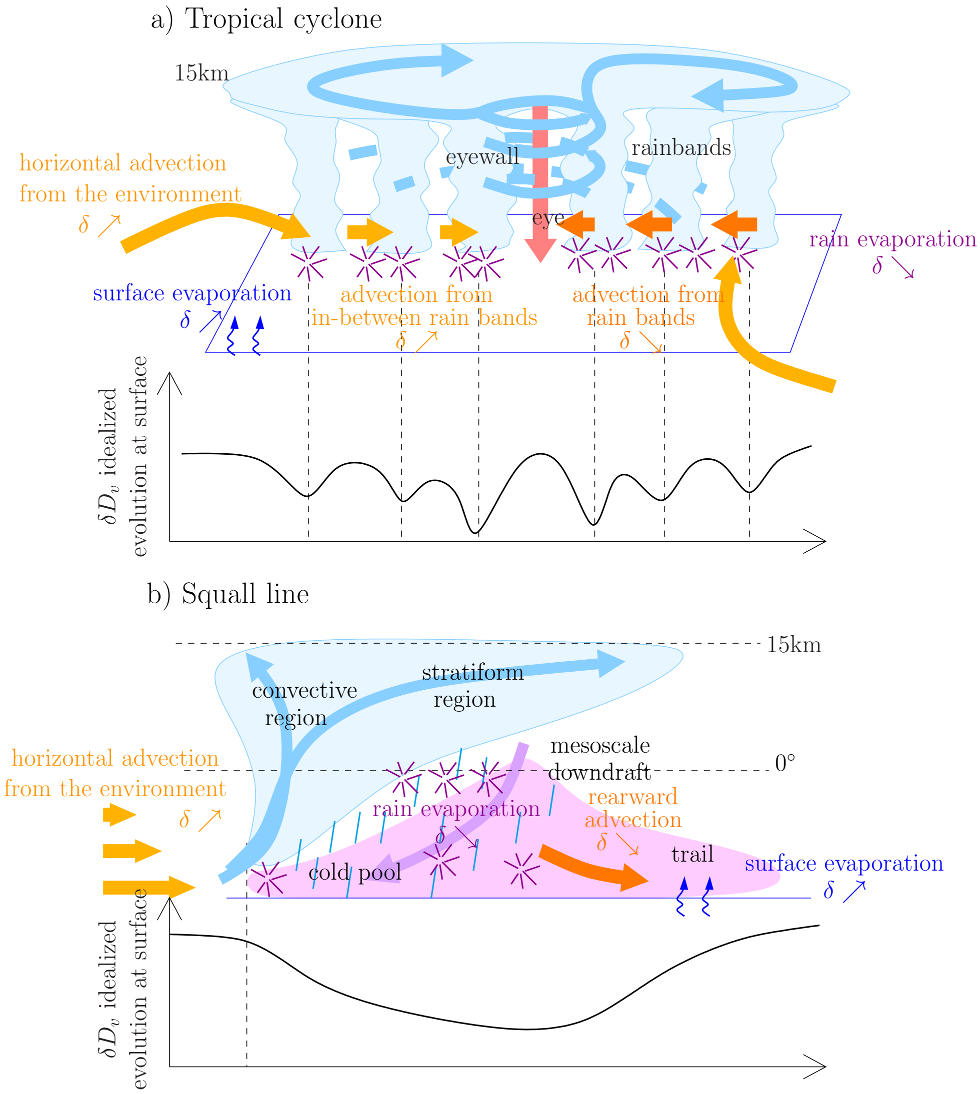

Figure 11. Schematic summarizing the processes controlling the water vapor composition inside tropical cyclones (a) and squall lines (b). The key driver is rain evaporation, indicated by purple stars. Rain evaporation deplete the water vapor in the rain bands and eyewall of tropical cyclones and in the convective and stratiform regions of squall lines. Horizontal advection then reshapes this pattern. Dark orange arrows indicate horizontal advection from depleted regions to less depleted regions, contributing to spread the depleted anomalies inward in cyclones and rearward in squall lines. Light orange arrows indicate horizontal advection from less depleted regions to depleted regions, limiting the depletion in most depleted regions.

frequency of large, long-lived, organized convective systems such as squall lines (Maupin et al., 2021).

However, when considering paleoclimate records at the annual scale or larger, the isotopic composition reflects an average over many convective systems of different organization types. In our simulations, this is equivalent to considering the domain-mean δD in simulations of tropical cyclones or squall lines relative to the domain-mean δD in simulations of isolated cumulonimbi, rather than the δD in tropical cyclone or squall lines relative to their environment in a given simulation. This paper focuses on mesoscale isotopic variations and does not discusses domain-mean values, because the realism of simulated mesoscale variations could be more easily assessed than the realism of domain-mean values. In particular, we realized that the domain-mean δD in the precipitation or water vapor of our tropical cyclone simulation was more enriched than that in simulations of squall lines or even of isolated cumulonimbi (Risi et al., 2020). This is at odds with observations of depleted cyclonic rains in the tropics (Lawrence et al., 2004). This discrepancy may be due to limitations in the radiative-convective equilibrium configuration. In radiative-convective equilibrium, the cyclone maintains a strong subsidence in its environment, which favors unrealistically dry conditions that allows enriched water vapor in the SCL to accumulate. In reality, tropical cyclones propagate and are thus not in equilibrium with their environment. Alternatively, this discrepancy may be due to the misinterpretation of the observations. In observations, the isotopic depletion associated with tropical cyclones could be blurred by the effects of average precipitation or large-scale circulation. To rigorously assess the role of convective organization, we would need to compare isotopic observations for different kinds of convective organization but for the same precipitation rate and large-scale context, as is now done for humidity (Tobin et al., 2012). This will be the subject of a future study. This will allow us to rigorously assess the realism of the domain-mean isotopic composition in our simulations, before possibly analyzing it in more detail.

Finally, when considering paleoclimate implications, how many other processes need to be investigated, including large-scale horizontal advection (Chen et al., 2021), land-atmosphere interactions along the air mass trajectories, infiltration processes, processes in the karstic systems and during calcite formation (Lases-Hernández et al., 2020). Our study is a first step towards a more comprehensive understanding of water isotopic variations, focusing only on purely convective processes.

Acknowledgments

This work was granted access to the HPC resources of TGCC under the allocation 2092 made by GENCI.

CR. CM. and FV. acknowledge the national french program INSU-LEFE for the funding of the SAM-iso proposal at the AO LEFE 2021. C.M. gratefully acknowledges funding from the European Research Council (ERC) under the European Union's Horizon 2020 research and innovation programme (Project CLUSTER, grant agreement No 805041). P.B. was supported by the National Science Foundation under Grant No. AGS-1938108.

G.V. contributed as part of his internship as a Master student at Sorbonne Universit, with a funding from Paris Sciences & Lettres "ANR-10-IDEX- 0001-02". C. D. contributed as part of her internship as a Bachelor student at Sorbonne Universit. S.A. contributed as part of her PhD, with a funding from Ecole Normale Suprieure de Paris-Saclay.

Information on SAM can be found on this web page: `http://rossby.msrc.sunysb.edu/~marat/SAM.html`. The simulation outputs used in this article have been submitted to the PANGEA data repository. The temporary link during the submission process is: `https://issues.pangaea.de/browse/PDI-29361`.

References

Aggarwal, P. K., Romatschke, U., Araguas-Araguas, L., Belachew, D., Longstaffe, F. J., Berg, P., . . . Funk, A. (2016). Proportions of convective and stratiform precipitation revealed in water isotope ratios. *Nature Geoscience*, *9*(8), 624-629, https://doi.org/10.1038/ngeo2739.

Baldini, L. M., Baldini, J. U., McElwaine, J. N., Frappier, A. B., Asmerom, Y., Liu, K.-b., . . . others (2016). Persistent northward north atlantic tropical cyclone track migration over the past five centuries. *Scientific reports*, *6*, 37522.

Biggerstaff, M. I., & Houze Jr, R. (1991). Kinematic and precipitation structure of the 10–11 june 1985 squall line. *Monthly weather review*, *119*(12), 3034–3065.

Blossey, P. N., Kuang, Z., & Romps, D. M. (2010). Isotopic composition of water in the tropical tropopause layer in cloud-resolving simulations of an idealized tropical circulation. *J. Geophys. Res.*, *115*, D24309, doi:10.1029/2010JD014554.

Bryan, G. H., & Morrison, H. (2012). Sensitivity of a simulated squall line to horizontal resolution and parameterization of microphysics. *Monthly Weather Review*, *140*(1), 202–225.

Caniaux, G., Redelsperger, J.-L., & Lafore, J.-P. (1994). A numerical study of the stratiform region of a fast mooving squall line. part 1: general description and water and heat budgets. *J. Atm. Sci*, *51*, 2046-2074.

Chakraborty, S., Sinha, N., Chattopadhyay, R., Sengupta, S., Mohan, P., & Datye, A. (2016). Atmospheric controls on the precipitation isotopes over the andaman islands, bay of bengal. *Scientific reports*, *6*(1), 1–11.

Chavas, D. R., & Emanuel, K. (2014). Equilibrium tropical cyclone size in an idealized state of axisymmetric radiative–convective equilibrium. *Journal of the Atmospheric Sciences*, *71*(5), 1663–1680.

Chen, F., Huang, C., Lao, Q., Zhang, S., Chen, C., Zhou, X., . . . Zhu, Q. (2021). Typhoon control of precipitation dual isotopes in southern china and its palaeoenvironmental implications. *Journal of Geophysical Research: Atmospheres*, e2020JD034336.

Chong, M. (2009). The 11 August 2006 squall line system as observed from MIT Doppler radar during the AMMA SOP. *Quart. J. R. Meteor. soc., this volume*.

Chong, M., & Hauser, D. (1990). A tropical squall line observed during the COPT81 experiment in West Africa: Part III: heat and moisture budgets. *Mon. Wea. Rev.*, *118*, 1696-1706.

Conroy, J. L., Noone, D., Cobb, K. M., Moerman, J. W., & Konecky, B. L. (2016). Paired stable isotopologues in precipitation and vapor: A case study of the amount effect within western tropical pacific storms. *Journal of Geophysical Research: Atmospheres*, *121*(7), 3290–3303.

Craig, H. (1961). Isotopic variations in meteoric waters. *Science*, *133*, 1702-1703.

Craig, H., & Gordon, L. I. (1965). Deuterium and oxygen-18 variations in the ocean and marine atmosphere. *Stable Isotope in Oceanographic Studies and Paleotemperatures*, *Laboratorio di Geologia Nucleate, Pisa, Italy*, 9-130.

Cruz, F. W., Vuille, M., Burns, S. J., Wang, X., Cheng, H., Werner, M., . . . Nguyen, H. (2009). Orbitally driven east?west antiphasing of South American precipitation. *Nature Geoscience*, *2*, 210-214.

Dansgaard. (1964). Stable isotopes in precipitation. *Tellus*, *16*, 436-468.

Field, R. D., Jones, D. B. A., & Brown, D. P. (2010). The effects of post-condensation exchange on the isotopic composition of water in the atmosphere. *J. Geophy. Res.*, *115, D24305*, doi:10.1029/2010JD014334.

Frappier, A. B., Sahagian, D., Carpenter, S. J., González, L. A., & Frappier, B. R. (2007). Stalagmite stable isotope record of recent tropical cyclone events. *Geology*, *35*(2), 111–114.

Fudeyasu, H., Ichiyanagi, K., Sugimoto, A., Yoshimura, K., Ueta, A., Yamanaka, M. D., … Ozawa, K. (2008). Isotope ratios of precipitation and water vapor observed in Typhoon Shanshan. *J. Geophys. Res.*, *113*, D12113, doi:10.1029/2007JD009313.

Gamache, J. F., & Houze, R. A. (1981). Mesoscale air motions associated with a tropical squall line. *monthly weather review*, *110*, 118-135.

Gamache, J. F., & Houze, R. A. (1983). Water budget of a mesoscale convective system in the tropics. *J. Atmos. Sci.*, *40*, 1835-1850, oi: http://dx.doi.org/10.1175/1520-0469(1983)040.

Gao, J., Masson-Delmotte, V., Risi, C., He, Y., & Yao, T. (2013). What controls southern Tibetan Plateau precipitation deltaO18 at seasonal and intra-seasonal scales? A case study at Lhasa and Nyalam. *Tellus*.

Gedzelman, S., Lawrence, J., Gamache, J., Black, M., Hindman, E., Black, R., … Zhang, X. (2003). Probing hurricanes with stable isotopes of rain and water vapor. *Mon. Wea. Rev.*, *131*, 112-1127.

Gentry, M. S., & Lackmann, G. M. (2010). Sensitivity of simulated tropical cyclone structure and intensity to horizontal resolution. *Monthly Weather Review*, *138*(3), 688–704.

Guilpart, E. (2018). *Etude de la composition isotopique (deutérium et oxygène 18) de la vapeur d'eau dans l'atmosphère sur l'île de la réunion: apport à la compréhension des processus humides atmosphériques en région tropicale.* Unpublished doctoral dissertation, Université Paris-Saclay (ComUE).

Houze, R. A. (2004). Mesoscale convective systems. *Rev. Geophys.*, *42 (4)*, DOI: 10.1029/2004RG000150.

Houze, R. A. (2010). Clouds in tropical cyclones. *Monthly Weather Review*, *138*(2), 293–344.

Jackisch, D., Yeo, B. X., Switzer, A. D., He, S., Cantarero, D. L. M., Siringan, F. P., & Goodkin, N. F. (2020). Precipitation stable isotopic signatures of tropical cyclones in metropolitan manila, philippines show significant negative isotopic excursions. *Natural Hazards and Earth System Sciences Discussions*, 1–26.

Jakob, C., Singh, M., & Jungandreas, L. (2019). Radiative convective equilibrium and organized convection: An observational perspective. *Journal of Geophysical Research: Atmospheres*, *124*(10), 5418–5430.

Khairoutdinov, M., & Emanuel, K. (2013). Rotating radiative-convective equilibrium simulated by a cloud-resolving model. *Journal of Advances in Modeling Earth Systems*, *5*(4), 816–825.

Khairoutdinov, M. F., & Randall, D. A. (2003). Cloud resolving modeling of the arm summer 1997 iop: Model formulation, results, uncertainties, and sensitivities. *Journal of the Atmospheric Sciences*, *60*(4), 607–625.

Kurita, N. (2013). Water isotopic variability in response to mesoscale convective system over the tropical ocean. *Journal of Geophysical Research*, *118(18)*, 10-376.

Lacour, J.-L., Risi, C., Worden, J., Clerbaux, C., & Coheur, P.-F. (2017). Isotopic signature of convection's depth in water vapor as seen from iasi and tes d observations. *Earth Planet. Sci. Lett.*, *7*, 9645-9663, doi.org/10.5194/acp-17-9645-2017.

Lases-Hernández, F., Medina-Elizalde, M., & Frappier, A. B. (2020). Drip water δ18o variability in the northeastern yucatán peninsula, mexico: Implications for tropical cyclone detection and rainfall reconstruction from speleothems. *Geochimica et Cosmochimica Acta*, *285*, 237–256.

Lawrence, J., & Gedzelman, S. (2003). Tropical ice core isotopes: Do they reflect changes in storm activity? *Geophys. Res. Lett.*, *30*, 44-1.

Lawrence, J. R. (1998). Isotopic spikes from tropical cyclones in surface waters: Opportunities in hydrology and paleoclimatology. *Chemical Geology*, *144*(1-2), 153–160.
Lawrence, J. R., & Gedzelman, S. D. (1996). Low stable isotope ratios of tropical cyclone rains. *Geophys. Res. Lett.*, *23*, 527-530. doi: 10.1029/96GL00425
Lawrence, J. R., Gedzelman, S. D., Dexheimer, D., Cho, H.-K., Carrie, G. D., Gasparini, R., ... Biggerstaff, M. I. (2004, March). Stable isotopic composition of water vapor in the tropics. *J. Geophys. Res.*, *109*, D06115, doi:10.1029/2003JD004046. doi: 10.1029/2003JD004046
Lawrence, J. R., Gedzelman, S. D., Gamache, J., & Black, M. (2002). Stable isotope ratios: Hurricane Olivia. *J. Atmos. Chem*, *41*, 67-82.
Lekshmy, P., Midhun, M., Ramesh, R., & Jani, R. (2014). 18 o depletion in monsoon rain relates to large scale organized convection rather than the amount of rainfall. *Scientific reports*, *4*, 5661.
Maupin, C. R., Roark, E. B., Thirumalai, K., Shen, C.-C., Schumacher, C., Van Kampen-Lewis, S., ... others (2021). Abrupt southern great plains thunderstorm shifts linked to glacial climate variability. *Nature Geoscience*, *14*(6), 396–401.
Medina-Elizalde, M., & Rohling, E. J. (2012). Collapse of classic maya civilization related to modest reduction in precipitation. *Science*, *335*(6071), 956–959.
Merlivat, L., & Jouzel, J. (1979). Global climatic interpretation of the Deuterium-Oxygen 18 relationship for precipitation. *J. Geophys. Res.*, *84*, 5029-5332.
Moerman, J. W., Cobb, K. M., Adkins, J. F., Sodemann, H., Clark, B., & Tuen, A. A. (2013). Diurnal to interannual rainfall δ18o variations in northern borneo driven by regional hydrology. *Earth and Planetary Science Letters*, *369*, 108–119.
Moore, M., Blossey, P., Muhlbauer, A., & Kuang, Z. (2016). Microphysical controls on the isotopic composition of wintertime orographic precipitation. *J. Geophys.l Res.*, *121*(12), 7235–7253.
Moore, M., Kuang, Z., & Blossey, P. N. (2014). A moisture budget perspective of the amount effect. *Geophys. Res. Lett.*, *41*, 1329-1335, doi:10.1002/2013GL058302.
Muller, C. (2013). Impact of convective organization on the response of tropical precipitation extremes to warming. *Journal of climate*, *26*(14), 5028–5043.
Muller, C. J., & Romps, D. M. (2018). Acceleration of tropical cyclogenesis by self-aggregation feedbacks. *Proceedings of the National Academy of Sciences*, 201719967.
Munksgaard, N. C., Zwart, C., Kurita, N., Bass, A., Nott, J., & Bird, M. I. (2015). Stable isotope anatomy of tropical cyclone ita, north-eastern australia, april 2014. *PloS one*, *10*(3), e0119728.
Nott, J., Haig, J., Neil, H., & Gillieson, D. (2007). Greater frequency variability of landfalling tropical cyclones at centennial compared to seasonal and decadal scales. *Earth and Planetary Science Letters*, *255*(3-4), 367–372.
Price, R. M., Swart, P. K., & Willoughby, H. E. (2008). Seasonal and spatial variation in the stable isotopic composition (δ18o and δd) of precipitation in south florida. *Journal of Hydrology*, *358*(3-4), 193–205.
Risi, C., Bony, S., Vimeux, F., Chong, M., & Descroix, L. (2010). Evolution of the water stable isotopic composition of the rain sampled along Sahelian squall lines. *Quart. J. Roy. Meteor. Soc.*, *136 (S1)*, 227 - 242.
Risi, C., Bony, S., Vimeux, F., Descroix, L., Ibrahim, B., Lebreton, E., ... Sultan, B. (2008). What controls the isotopic composition of the African monsoon precipitation? Insights from event-based precipitation collected during the 2006 AMMA campaign. *Geophys. Res. Lett.*, *35*, doi:10.1029/2008GL035920. doi: 10.1029/2008GL035920
Risi, C., Muller, C., & Blossey, P. (2021). Rain evaporation, snow melt, and en-

trainment at the heart of water vapor isotopic variations in the tropical troposphere, according to large-eddy simulations and a two-column model. *Journal of advances in modeling earth systems*, *13*(4), e2020MS002381.

Risi, C., Muller, C., & N, B. P. (2020). What controls the water vapor isotopic composition near the surface of tropical oceans? results from an analytical model constrained by large-eddy simulations. *Journal of Advances in Modeling Earth Systems*.

Robe, F. R., & Emanuel, K. A. (2001). The effect of vertical wind shear on radiative–convective equilibrium states. *Journal of the atmospheric sciences*, *58*(11), 1427–1445.

Rotunno, R., Klemp, J. B., & Weisman, M. L. (1988). A theory for strong, long-lived squall lines. *Journal of Atmospheric Sciences*, *45*(3), 463–485.

Sanchez-Murillo, R., Durán-Quesada, A. M., Esquivel-Hernández, G., Rojas-Cantillano, D., Birkel, C., Welsh, K., . . . others (2019). Deciphering key processes controlling rainfall isotopic variability during extreme tropical cyclones. *Nature communications*, *10*(1), 1–10.

Sinha, N., & Chakraborty, S. (2020). Isotopic interaction and source moisture control on the isotopic composition of rainfall over the bay of bengal. *Atmospheric Research*, *235*, 104760.

Skrzypek, G., Dogramaci, S., Page, G. F., Rouillard, A., & Grierson, P. F. (2019). Unique stable isotope signatures of large cyclonic events as a tracer of soil moisture dynamics in the semiarid subtropics. *Journal of Hydrology*, *578*, 124124.

Su, H., Bretherton, C. S., & Chen, S. S. (2000). Self-aggregation and large-scale control of tropical deep convection: A modeling study. *Journal of the atmospheric sciences*, *57*(11), 1797–1816.

Tan, J., Jakob, C., & Lane, T. P. (2013). On the identification of the large-scale properties of tropical convection using cloud regimes. *Journal of Climate*, *26*(17), 6618–6632.

Taupin, J.-D., & Gallaire, R. (1998). Variabilit isotopique I'chelle infra-vnement de quelques pisodes pluvieux dans la rgion de Niamey, Niger. *C.R. Acad. des Sciences*, *326*, 493-498.

Thompson, G., Field, P. R., Rasmussen, R. M., & Hall, W. D. (2008). Explicit forecasts of winter precipitation using an improved bulk microphysics scheme. part ii: Implementation of a new snow parameterization. *Monthly Weather Review*, *136*(12), 5095–5115.

Tobin, I., Bony, S., & Roca, R. (2012). Observational evidence for relationships between the degree of aggregation of deep convection, water vapor, surface fluxes and radiation. *Journal of Climate*.

Torri, G., Ma, D., & Kuang, Z. (2017). Stable water isotopes and large-scale vertical motions in the tropics. *J. Geophys. Res*, *122(7)*, 3703-3717.

Tremoy, G., Vimeux, F., Mayaki, S., Souley, I., Cattani, O., Favreau, G., & Oi, M. (2012). A 1-year long delta18O record of water vapor in Niamey (Niger) reveals insightful atmospheric processes at different timescales. *Geophys. Res. Let.*.

Tremoy, G., Vimeux, F., Soumana, S., Souley, I., Risi, C., Cattani, O., . . . Oi, M. (2014). Clustering mesoscale convective systems with laser-based water vapor delta18O monitoring in Niamey (Niger). *J. Geophys. Res.*, *119(9)*, 5079-5103, DOI: 10.1002/2013JD020968.

Vimeux, F., Gallaire, R., Bony, S., Hoffmann, G., & Chiang, J. C. H. (2005, December). What are the climate controls on deltaD in precipitation in the Zongo Valley (Bolivia)? Implications for the Illimani ice core interpretation. *Earth Planet. Sci. Lett.*, *240*, 205-220. Retrieved from http://adsabs.harvard.edu/cgi-bin/nph-bib_query?bibcode=2005E%26PSL.240..205V&db_key=AST doi: 10.1016/j.epsl.2005.09.031

Vimeux, F., Tremoy, G., Risi, C., & Gallaire, R. (2011). A strong control of the South American SeeSaw on the intraseasonal variability of the isotopic composition of precipitation in the Bolivian Andes. *Earth. Planet. Sci. Lett.*, *307 (1-2)*, 47-58.

Wang, Y. J., Cheng, H., Edwards, R. L., An, Z. S., Wu, J. Y., Shen, C. C., & Dorale, J. A. (2001). A high-resolution absolute-dated late Pleistocene Monsoon record from Hulu Cave, China. *Science*, *294(5550)*, 2345-8.

Worden, J., Noone, D., & Bowman, K. (2007). Importance of rain evaporation and continental convection in the tropical water cycle. *Nature*, *445*, 528-532.

Xu, T., Sun, X., Hong, H., Wang, X., Cui, M., Lei, G., ... Jiang, X. (2019). Stable isotope ratios of typhoon rains in fuzhou, southeast china, during 2013–2017. *Journal of Hydrology*, *570*, 445–453.

Yang, M.-H., & Houze Jr, R. A. (1995). Sensitivity of squall-line rear inflow to ice microphysics and environmental humidity. *Monthly weather review*, *123*(11), 3175–3193.

Zipser, E. (1977). Mesoscale and convective scale downdrafts as distinct components of squall-line structure. *Mon. Wea. Rev.*, *105*, 1568-1589.